LBL-29659

Lawrence Berkeley Laboratory
UNIVERSITY OF CALIFORNIA

Materials & Chemical
Sciences Division

Morphological Studies of Lithium Fluoride Surfaces

J.W. Bullard
(M.S. Thesis)

September 1990

Prepared for the U.S. Department of Energy under Contract Number DE-AC03-76SF00098

DISCLAIMER

LBL-29659

MORPHOLOGICAL STUDIES OF LITHIUM FLUORIDE SURFACES

Jeffrey Wayne Bullard

Master of Science Thesis

September 1990

Materials Science Division
Lawrence Berkeley Laboratory
and Department of Materials Science and Mineral Engineering
University of California
Berkeley, California 94720

This work was supported by the Director, Office of Energy Research, Office of Basic Energy Science, Materials Sciences Division of the U.S. Department of Energy under Contract Number DE-AC03-76SF00098.

Table of Contents

I. Introduction 1
A. Theory 2
1. Thermodynamic Considerations 2
2. Kinetic Considerations 5
B. Experimental Observations 7

II. Experimental Procedures 10
A. Profile Decay Studies 10
B. Particle Shape Studies 13

III. Results and Discussion 15
A. Profile Decay Studies 15
B. Particle Shape Studies 23
1. Isolated particles and small agglomerates 23
2. Bulk powder compacts 25

IV. Summary 29

Appendix 31

Tables 32

Figures 36

I. Introduction

From equilibrium thermodynamic considerations, one would expect most partially sintered ceramic materials to exhibit faceted surfaces since they usually have highly anisotropic surface tension [1]. However most theories incorporating kinetic arguments, such as sintering models, assume isotropic surface tensions and therefore predict rounded microstructures. This assumption is consistent with the observation that partially sintered ceramic microstructures are commonly composed of mostly rounded particles [2],[3],[4],[5].

On the other hand, faceted shapes sometimes also are observed for particles during sintering [2],[3], and for cavities during studies of pore-grain boundary interactions [6], equilibrium cavity shapes [7],[8],[9], and crack healing [10],[11]. This study was undertaken in an effort to clarify the conditions under which faceted surfaces may be present during shape changes of crystalline ceramics.

Lithium fluoride, which is chemically inert and which was available in relatively large, pure crystals, was chosen for study of the features that mimic the necks present during sintering. Square wave profiles were introduced into {100} surfaces of lithium fluoride by means of a photolithography/ion-beam-milling technique, which has recently been used for this purpose by Bennison and Harmer [12]. The evolution of the profile at elevated temperatures was studied, the purpose being to study the morphological evolution of the profiles and, if possible, to identify the rate limiting step in the process.

In related experiments, changes in the morphology of isolated lithium fluoride particles, of small clusters of lithium fluoride particles, and of an aggregate of lithium fluoride particles were observed under near-equilibrium conditions.

These studies were undertaken to evaluate the roles of thermodynamics and kinetics in determining surface morphologies of lithium fluoride, to identify some of the experimental factors affecting these morphologies, and to evaluate the effects of these factors.

A. Theory

1. Thermodynamic Considerations

The theoretical foundation for determining equilibrium crystal shapes was set forth by Gibbs [13] and Curie [14]. They independently predicted the condition of equilibrium for a crystal with respect to any reconfiguration of the atoms:

$$\sum_{i=1}^{n} \gamma_i A_i \quad \text{is a minimum,} \tag{2}$$

where γ_i represents the work to form a unit area of the ith crystal face, and A_i represents the area of the ith crystal face. The quantity γ has the units of energy per unit surface area, or alternatively force per unit distance as discussed by Adamson [15], where he calls γ the surface tension. Both Mullins [16] and Herring [17] have also called γ the surface tension, and that term will be used here as well. As discussed by Mullins, Wulff deduced the following corollary relation from Eq. (2):

$$\gamma_1 / R_1 = \gamma_2 / R_2 = \ldots = \gamma_i / R_i \tag{3}$$

where R_i is the perpendicular distance from the center of symmetry (alternately called the Wulff point) to the ith surface [16].

For a crystalline solid, γ will generally depend on the orientation of the surface considered. The orientation can be described in terms of a unit vector, $\hat{n}$, normal to the surface. The quantity γ can then be expressed as the function $\gamma(\hat{n})$. Alternatively, the orientation dependence can be expressed as $\gamma(\theta)$ where θ is the angle between $\hat{n}$ and some reference unit normal.

The geometric construction known as the Wulff construction is based on equation (3), and is used to obtain the equilibrium shape of a crystal. First, a polar plot of $\gamma(\theta)$ is made. Then a line is drawn from the origin of the plot to each point on the γ-"surface". A plane normal to each line at the γ-surface is then constructed, and the inner envelope of the planes defines the equilibrium shape.

Equation (3) and, therefore, the Wulff construction assumes that the volume of the crystal is constant. For nonequilibrium particle shapes, or for a collection of particles, shape changes which reduce the summation of Eq. (2) are allowed, where the summation now includes grain boundary terms as well [18].

It is apparent from the Wulff construction that the equilibrium shape of a crystal may consist wholly of faceted surfaces, wholly of curved surface, or a combination of the two, depending on the local anisotropy of the surface. Over the orientations for which a smoothly curved surface is observed, the surface tension is isotropic or nearly so.

Cahn and Hoffman introduced a vector formalism as an alternative to the scalar function $\gamma(\hat{n})$ [19] and also applied this formalism to curved and faceted surfaces to determine the equilibrium shape of an isolated particle of fixed volume [20].

Winterbottom determined the equilibrium shape of an isolated particle in contact with a foreign substrate [21]. To do so he assumed that the substrate and the substrate-particle interface are coplanar. He also assumed: 1) that particle-substrate interactions are short range, 2) that chemical potentials are fixed for each species present, and 3) that particle sizes fall in a range between 0.01 and 1.0 microns. The lower limit, which was established by Hirth and Pound [22], is the order of magnitude of particle dimensions at which edge and corner energies begin to influence the equilibrium shape. The upper limit, which was established by Herring [23], is a practical kinetic limit due to a driving force limitation to shape changes in large particles.

Winterbottom also points out that in order to determine the equilibrium shape of a free particle from that of a corresponding particle in contact with a substrate, the Wulff point must be located within the particle. This requirement is met if the specific interfacial free energy (or interfacial tension) of the particle-substrate interface is low.

Rottman and Wortis have used model calculations to determine the equilibrium shape of a two-dimensional crystallite embedded in another crystalline material at temperatures above absolute zero [24]. They were able to evaluate the influence of entropy effects, including the effect of entropy of ledge disorder in causing the 'surface roughening' phenomena predicted by Frank, Burton, and Cabrerra [25]. Sundquist also discussed the effect of surface entropy on the surface tension anisotropy, and concluded that the surface entropy contribution causes sharp edges and corners on the equilibrium shape to become rounded [26].

Experimental methods for determining the surface energy anisotropy of a material are necessary to obtain a polar γ-plot and thus predict the equilibrium shape. Sundquist has determined the anisotropy of surface energy for gold, silver, copper, nickel, and iron by examining the equilibrium shape of particles and then constructing a polar γ-plot based on the Wulff relation, Equation 3 [27].

Heyraud and Metois have studied the equilibrium shape of gold [28] and indium [29] particles in contact with a single crystal graphite substrate, and have determined the surface energy anisotropy in a manner like that used by Sundquist [26].

2. Kinetic Considerations

Measurement of the decay of a sinusoidal profile on a single crystal surface is an established means of studying material transport on and near the surface of metals. Mullins has set forth a theoretical model that incorporates both surface diffusion and bulk diffusion as possible transport mechanisms and provides the following equation for the shape of the surface as a function of time:

$$u(x,t) = a\exp[-(C\omega^3 + B\omega^4)t]\sin\omega x \qquad (1)$$

where a is the amplitude, ω is the wave number $(2\pi/\lambda)$, x is the position along an axis parallel to the mean surface, and B and C are material and temperature dependent constants for surface and bulk diffusion, respectively [16].

The primary assumption invoked in this analysis is that diffusion of atoms to surface sites is the rate limiting step in the process. This assumption allows the rate of decay to be described in terms of the Nernst-Einstein diffusion equation and allows the surface growth step to be neglected.

An important prediction of this analysis is that any periodic profile (not only sine waves) will decay into a sinusoidal profile and then decay according to the above equation. Consequently, the profile shape is not critical as long as it is periodic, and an investigator has considerable flexibility in the introduction of profiles into the surface. In fact, as Blakely has shown, a single scratch in a surface can be used for this type of study, although considerable approximation must be used in the analysis [30].

Blakely, Bonzel and others [30],[31],[32],[33],[34] have conducted profile decay studies on a variety of metal surfaces, and have found excellent agreement with Mullins' model. In their studies, they suppressed bulk diffusion so that only surface diffusion is significant, and on this basis calculated surface diffusion coefficients and activation energies.

It has been suggested [35] that it may be possible to determine the rate limiting step in the filling of faceted channels by means of a technique similar to the one described above. By systematically varying the distance between channels and studying the rate of filling, one could in principle distinguish between diffusion and the possibly slow addition or subtraction of new layers to the low index facets as rate limiting steps. If the profile were to remain faceted throughout, then this determination would be straightforward. In a range of conditions for which ledge growth is limiting, the rate of filling should be dependent on channel width, but insensitive to the distance between channels. However, if the profile were to smooth into a sine wave, then the growth of new faceted layers could not be rate limiting, and only diffusion data could be obtained.

B. Experimental Observations

Metal particles, even under near-equilibrium conditions, usually have largely rounded surfaces, at least at temperatures high enough for mass transport measurements [27],[28],[29]. But sharply faceted metal particles have sometimes been observed for the same or similar metals under nominally similar conditions [36],[37]. The faceting is probably a consequence of oxygen adsorption [27].

For NaCl-type ionically bonded solids only {100} surfaces are electrically neutral, assuming no surface relaxation or reconstruction. The neutral {100} surfaces are thermodynamically favored and have been observed during sintering [38],[11] and studies of equilibrium pore shapes [7].

While the equilibrium shapes of free particles and those of particles in contact with a foreign substrate have been treated both theoretically and experimentally, the matter of the crystal shapes in powder compacts and even of small agglomerates has received less attention. In fact, the conditions under which crystals facet have not been established to the extent that predictions can be made with certainty. In addition, the experimental work has been performed almost exclusively on metals. Nonmetallic free particles, agglomerates, and compacts sometimes have rounded and sometimes faceted particles. The conditions that determine which have not been explained. Studies on MgO, CoO, and LiF illustrate the kind of observations which have been made.

Mikijelj and Whittemore found that 0.2 μm diameter particles of $MgO\text{-}MgCl_2(1\%)$ exhibited marked {100} faceting and coarsening when sintered in dry argon at temperatures exceeding 1173°C. However, when the sintering was performed in vacuum, the faceting did not occur, leading to the conclusion that faceting

occurred via an evaporation-condensation transport mechanism which was accelerated by a volatile chloride species [2]. These results also suggest that faceting is a near-equilibrium phenomenon since an argon atmosphere promotes near-equilibrium vapor pressure while a continuously evacuated environment represents far-from-equilibrium conditions.

Kim, Dahmen, and Searcy decomposed $Mg(OH)_2$ in vacuum to form MgO as aggregates of particles which had the shapes of orthorhombic boxes with edges of 0.8 to 3 nm. During sintering in vacuum at 1250°C or in water vapor at 600° C, coarsening occurred, and the faceted shapes were retained. For MgO under these conditions, vapor transport cannot be significant [3].

Kumar and Johnson reported that 15 to 20 μm spheres of CoO facet immediately during the first 1% of densification [39].

Wang, Harmer, and Chou observed isolated pores in LiF and reported that the quasi-equilibrium shape is cubic with {111} truncation of the corners and {110} truncation of the edges. The investigators also observed that when the pores were annealed in air at 780°C ($0.94T_m$) the smaller pores (~1 μm) had almost perfectly square cross sections while the larger ones (~10 μm) assumed rectangular shapes. Gaseous adsorption of O_2 or H_2O was suggested to be responsible for the lowering of the {100} surface tension [7]. The rectangular shapes of the larger pores are most likely metastable [19].

Raj and co-workers studied crack healing in LiF and observed pronounced {100} faceting of the crack tips at temperatures as high as 760°C ($0.92T_m$) [11]. With the crack tip width held constant at 0.40 μm, these investigators asserted that surface diffusion was the dominant sintering mechanism below 700°C while volume diffusion

dominated above this temperature. By varying the crack tip width they observed that the sintering rate was independent of tip width for surface diffusion, while for volume diffusion, the sintering rate varied inversely with crack tip width.

II. Experimental Procedures

A. Profile Decay Studies

Lithium fluoride crystals with dimensions 25 mm x 25 mm x 1 mm were obtained[a]. As received, the crystals were 99.9 % pure and their (100) faces were polished to 0.1 μm. A detailed chemical analysis is given in the appendix.

The photolithography/ion-beam milling technique used to produce the desired surface features follows closely that described by Roedel [6] and will be only briefly described here.

The pattern to be exposed consisted of a series of 6 mm-long parallel channels, the cross sections of which were of varying widths and spacings. The pattern was generated on KIC, a CAD system in UNIX, and transferred to a square 64 mm x 64 mm chrome-coated glass mask. The mask layout is shown schematically in Figure 1.

The as-received crystals were washed in anhydrous methanol and blown dry with nitrogen to remove any remnant surface films or contaminants from the polishing process. Next, a thin, even coating of photoresist[b] was applied to the crystal by spinning eight drops at 5000 rpm for 30 s. The resulting photoresist thickness was measured on similar specimens using a profilometer[c] and was found to be ≈1.0 μm. The crystal was then soft-baked on a covered hot plate at 95°C for 25 min.

The crystal and mask were next aligned and exposed in a 4:1 projection printer[d] so that the faces of the profile were of {100} orientation (±≈ 1°). During the exposure

---

[a]Englehard Company, Solon, Ohio

[b]Shipley 1400:31, Shipley Co., Inc., Santa Clara, California.

[c]Alphastep AS200, Tencor, Mountain View, California.

[d]Canon Wafer Stepper, Canon, Santa Clara, California.

step the pattern on the mask was reduced by a factor of four and transferred to the photoresist. After exposing the crystal for approximately 1.5 s, the photoresist was developed by immersion in a 1:1 developer[e] concentrate/distilled water solution for 30 s, rinsed by immersion in water for 15 s, and then blown dry with a nitrogen gun. The crystal was then hard-baked at 120°C for 25 min on a covered hot plate.

The developing process resulted in channels which were wider and in spaces between channels which were narrower than those on the mask. This is due at least in part to overexposure. Another possible contribution to channel widening is "lateral" development, in which the photoresist is developed and removed in the lateral direction as well as normal to the crystal surface. These phenomena are difficult to prevent. However, the specific dimensions of the profiles are not important because the dimensions left in the LiF after processing were measured by scanning electron microscopy.

In order to introduce the exposed pattern into the LiF, the crystal and photoresist were milled[f] with an argon ion beam for 12 to 20 min. The milling parameters used are listed in Table 1.

The remaining photoresist was removed in several steps. First, the crystal was cleaned for 2 min in 1,1-trichloroethane to remove the silver paste. Second, the crystal was cleaned in resist remover (active ingredient n-methyl 2-pyrrolidone)[g] to remove most of the photoresist. The crystal was then again cleaned in trichloroethane for 5 min to remove any remnant resist and to rinse off the remover. Lastly, the crystal was

[e]Microposit Developer, Shipley Co., Inc.

[f]Veeco Microetch System, Veeco Instruments Inc., New York, New Jersey.

[g]Microposit Resist Remover, Shipley Co., Inc.

cleaned in anhydrous methanol for another five minutes to remove the 1,1-trichloroethane. All cleaning steps were performed ultrasonically. After cleaning, the specimen was blown dry with a nitrogen gun.

At this point, each crystal contained four etched patterns on its surface. The crystal was therefore sectioned into quarters by cleaving or diamond sawing so that each pattern could be heat treated independently.

The crystals were annealed at 550°C for 15 h to remove surface contaminants and to relieve stresses caused by the processing steps. Following the anneal, the crystals were heat treated at temperatures between 680° and 770°C ($0.81T_m$ and $0.91T_m$ respectively) for varying time intervals. In order to prevent free evaporation and to achieve near-equilibrium conditions, two precautions were taken. First, the furnace chamber was evacuated to a pressure of 10^{-6} Torr and then back-filled with 99.98% pure argon at one atmosphere pressure. Since water may adsorb on the surface of LiF, the argon was passed through a filter of dessicant[h] to remove water before being introduced into the furnace chamber. Second, a flat lithium fluoride crystal was positioned ≈1 mm above the profile. This arrangement which should establish a near-equilibrium vapor pressure at the profile surface is shown in Figure 2.

Following the annealing period, the crystals were cooled in one of two ways. One cooling treatment consisted of immediately removing the crystal from the furnace and exposing it to room temperature. This process took ~5 s to perform and will be referred to as a *quench* in the following discussion. The other cooling treatment consisted of turning the furnace power off and letting the crystal cool down within the furnace. The

[h]Drierite, VWR Scientific, San Francisco, California.

initial cooling rate was 20°C/min (for a 770°C annealing temperature) and gradually decreased as the furnace temperature decreased. From now on, this cooling treatment will be called *slow*.

After the heat treatment, the crystal was cut normal to the profile surface and mounted so that the profile cross-sections could be studied directly in a scanning electron microscope[i]. Photomicrographs representing a large sample of each of the profiles were collected. The dimensions of the profiles were then measured using an image analyzer[j]. When possible, five or six measurements were recorded so that a mean and standard deviation of the measurement was obtained.

B. Particle Shape Studies

The material used in this study was lithium fluoride powder [k] of 99.9% purity. A more detailed chemical annalysis of the powder is given in the appendix. Microscopic examination showed the particles to be approximately cubic with ~ 2 μm cube edge lengths.

To study the shapes that particles approached when annealed in isolation, in small agglomerates, and in bulk compacts, the following procedure was developed.

A 0.04 volume percent powder suspension was prepared by adding the appropriate amount of powder to 20 ml of ethanol and three drops of concentrated hydrochloric acid as a deflocculating agent to minimize agglomeration. One drop of

[i]ISI WB-6, International Scientific Instruments, Inc., Milpitas, California.
[j]IBAS 2000.
[k]Johnson Matthey, Materials Technology, England.

this suspension was then applied to a 0.5 cm^2 single crystal graphite chip. Single crystal graphite was chosen as a substrate material because of its low surface tension in the hexagonal plane.

A graphite Knudsen effusion cell (1.5 cm in diameter, 2 cm in height, with a 0.5 mm orifice in the lid) was approximately three-quarters filled with the same powder used in the suspension. After the ethanol had evaporated from the graphite chip, the chip was positioned on top of the bulk powder and the effusion cell was capped. This arrangement is shown in Figure 3.

The prepared cell was heated in a vacuum of 10^{-6} torr to temperatures between 80 and 100% of the LiF melting point for varying times. The presence of the bulk powder bed assured an equilibrium vapor pressure within the cell and, therefore, minimal evaporation of the particles on the substrate.

The shapes of the particles and agglomerates on the substrate, as well as the morphology of the bulk compact, were studied before and after the heat treatment by scanning electron microscopy[1].

[1]ISI WB-6.

III. Results and Discussion

A. Profile Decay Studies

Before discussing the results of these experiments it is convenient to introduce the notation that will be used in the analysis.

A *profile* will be defined as a periodic array of parallel channels of constant width and spacing which is formed in a {100} surface of an LiF single crystal. A *specimen* will be defined as a portion of the single crystal which was subjected to a specified annealing treatment. Each specimen contains ten different profiles. Each *crystal* contains four specimens, as discussed in the previous section.

An individual profile will be specified by its intended channel width, w, and its intended channel spacing, d, in the following manner: ' w/d'. By 'intended' it is meant the dimensions designed into the mask. Figure 4 schematically illustrates these features.

Several dimensions of the profiles will be analyzed in the discussion. Unless otherwise specified, these dimensions were measured with reference to the bottom of the channel walls. In instances where the profiles rounded, the references are the inflection points of the profile (at the positive/negative curvature transition). The profile depth was measured from the top of a neighboring ridge to the appropriate reference. The cross sectional areas beneath the ridges were also measured as shown in Figure 4. In addition, some measurements were taken on the channels, while others were taken on the channel spacings. Which of these was measured will be indicated where appropriate.

Representative morphologies of the 'initial' profiles (following the first anneal at 550°C for 15 h in vacuum) are shown in Figure 5. The depths of the profiles are listed in Table 2. The cross sectional areas beneath the ridges for some of the profiles are listed in Table 3.

There are several points to be discussed concerning these initial profiles. First, as indicated in Table 2, the profile depths are not uniform. Specifically, the profiles with the widest channel spacing are the deepest, while those with progressively narrower spacings are progressively shallower. Measurements on each subsequently annealed profile are analyzed with reference to the measurements of the same profile, so the non-uniformity in depth is unimportant.

Second, the profiles are not perfectly rectangular. The walls of the channels slope in somewhat (up to ~30°) , and there is some rounding of the corners. This configuration, which results in some high energy surfaces compared to the desired {100} type, is caused by the ion-beam milling procedure. The effect, which has been reported by other investigators [40],[41], appears to be unavoidable under normal conditions.

Profiles on a specimen that was annealed at 770°C ($0.93T_m$) for 4 h and then rapidly quenched to room temperature (≈5 s) are shown in Figure 6. Note that the profiles smoothed considerably compared to their initial geometries. All corners have rounded significantly to the point that the profiles approximate sinusoidal waves. This behavior is predicted at least qualitatively by the diffusion-limiting analysis proposed by Mullins and therefore indicates that diffusion to surface sites may be the rate-limiting step in the process [16].

Additional support for this conclusion is given by the dependence of depth change on channel separation. The depths of the profiles and their changes relative to the initial profiles are listed in Table 2. The cross sectional areas beneath the ridges between inflection points and their relative changes are given in Table 3.

It is apparent immediately from the figures and the tables that the depth of the rounded channels is substantially reduced from the depths of the faceted channels observed after the 550°C anneal. This depth change depends in part on the profile geometry. For constant channel width, the mean depth decrease was greater for profiles with narrow channel separations, although exceptions can be found in Table 2. The standard deviation reported for these measurements is small enough so that the results can be interpreted with high confidence.

Table 3 indicates that the cross sectional area under the ridges between channels also decreased markedly during the second anneal. The mean change in cross sectional area of the ridges seems to be greater for large separation distances. However, since the standard deviation in these measurements is large, little confidence should be assigned to any geometry-dependent trends.

Crystal growth occurs by attachment at kink sites and advancement of ledges. Since smoothly rounded surfaces have a continuous variation in crystallographic orientation, they presumably possess a high concentration of these growth sites compared to highly faceted surfaces. It is therefore reasonable to assume that the presence of faceted surfaces indicates a slow growth step in profile decay, while rounded surfaces indicate that diffusion is rate limiting.

It is also possible that these results could be caused by a net loss of LiF from evaporation from kink sites (located predominantly at the profile corners) rather than

by a filling of the channels caused by diffusion. But free evaporation is unlikely to be the cause of the rounding for two reasons. First, precautions were taken to eliminate losses by free evaporation. As indicated in Section II, a single crystal of lithium fluoride was placed directly above the specimen surface in order to maintain near-equilibrium vapor pressure locally. To suppress evaporation further, the furnace chamber was back-filled with an argon atmosphere.

Evidence that loss of LiF from the surfaces examined is unlikely is found in Tables 2 and 3. The depth and cross sectional area changes of profiles 5/25 and 10/100 were measured for the channel rather than for the ridges (channel separation regions). Since the shoulder-to-floor depth and shoulder-to-shoulder cross sectional area of void space both decrease, a transfer of matter to the channel is indicated. If loss of LiF from the surface was the cause of the profile evolution, then presumably no net transfer of mass to the channel would be found; hence while vaporization between the nearby surfaces may contribute to the mass transport, a loss of LiF from the surfaces under study is ruled out.

Figure 7 shows profiles that were observed after an anneal at 770°C for 4 h in an argon atmosphere. In this run, however, the specimen was allowed to cool slowly to room temperature (20°C/min initially and progressively slower as temperature decreased). It is apparent from these figures that the treatment produces marked faceting in the {100} planes. Since rounding occurs at 770°C, it is apparent that the faceted profiles evolve from the rounded profiles during cooling. In all examples observed, these reconfigured profiles are more sharply faceted than the initial profiles.

There are several possible explanations for the re-faceting phenomenon. First, at high homologous temperatures entropy effects can cause cusps in the γ-plot to be

less pronounced [27]. This implies a decrease in the surface tension anisotropy with temperature increase, and therefore rounding may be expected at high temperatures whereas faceting may occur at lower temperatures. The sharpening of the γ-plot and therefore the rounding/faceting transition would be expected to occur gradually with temperature.

Second, surface melting at temperatures below the bulk melting temperatures could cause a rounding/faceting transition. Melting of the first few atomic layers on {110} surfaces of large lead crystals has been observed at temperatures as much as 40°C (7%) below the melting temperature [42]. If this effect is responsible for the re-faceting phenomenon then the transition may be expected to occur sharply within a few Kelvin as the surface layers solidify upon cooling.

The possible difference between the abruptness in transition between faceted and rounded crystals which could result from the two proposed mechanisms made experiments on the rounded-to-faceted transition of particular interest. A specimen was first annealed as before and quenched to form rounded profiles. It was then annealed at 725°C for 4 h in an argon atmosphere and again quenched. A sampling of the resultant profiles is given in Figure 8. The profiles are still rounded, roughly to the same degree as after the higher temperature anneal. The depth changes and cross-sectional area changes are tabulated in Tables 4 and 5, respectively.

In another experiment, a specimen was first annealed at 770°C for 4 h in argon and was then slowly cooled (again 20°C/min) to 725°C, and then quenched immediately from 725°C to room temperature. Representative micrographs of the resultant profiles are shown in Figure 9. Here the profiles are again rounded.

The first of these experiments suggests that a rounded morphology is stable at and above 725°C, but it may be that the profile is kinetically prevented from rearranging to a more stable faceted structure at this temperature. However, the second experiment confirms that the rounded-to-faceted transition occurs somewhere below 725°C. The exact temperature range over which this transition occurs has not yet been identified.

Similar experiments were performed on specimens that were ion-milled for 20 min. Figure 10 displays some of the initial profiles. Because the milling time was increased, the depths of the profiles are greater than those in the previous experiments, as can be seen in Table 6. In addition, the widths and spacings of the channels are somewhat different due to different exposure conditions.

A specimen of the type described above was annealed at 770°C in argon for 8 h and then slowly cooled to room temperature. The profile shapes are indicated in Figure 11. The profile depth changes are given in Table 6. Since the profiles did not refacet during the cooling period, it is suspected that the greater depth (approximately twice that of the previous profiles) presents a kinetic barrier to refaceting.

The same specimen was then annealed at 730°C for 16 h and slowly cooled to room temperature. The resultant profiles were markedly faceted as can be seen in Figure 12. The faceting presumably occurred during the cooling period since previous experiments suggest that faceted profiles are not stable above 725°C. The depth changes that occurred during the second anneal are given in Table 7 for a similarly prepared specimen.

The rounding/faceting transition appears to be reversible, since the initial (faceted) profiles were made to round and then refacetted. However as Figures 5 and

10 show, the original facets were not all of the {100} type as they are after refaceting. It is possible that the {100} surfaces formed after refaceting occur at a deep, low-energy cusp on the Wulff plot and therefore may not round again at higher temperature.

On the other hand, many of the initial profile surfaces were at least nearly of the {100} type, so that they were composed of {100} terraces and steps. Furthermore, the tops of the ridges were almost exclusively {100} planes. Since even these surfaces rounded at higher temperature, it is strongly suggested that the transition is reversible. A conclusive test would be to anneal a refacetted specimen at 770°C where the initial profiles rounded. This work is to be completed in the near future.

Examination of Tables 2-6 shows that while depths and areas of the rounded channels are reduced for the various geometries used, fluctuations in the data are large and no systematic variation with channel width, ridge width or their ratio can be determined.

The fluctuations may arise because of variations in the concentration of the screw dislocations which intercept the surfaces. Diffusion is usually assumed to be rate limiting in sintering and in related processes such as pore migration. But studies on pore migration in LiF indicate that since dislocations are potential ledge growth sites, a fluctuating dislocation concentration can lead to erratic ledge growth rates in faceted channels [7].

If it is assumed that the rounded profiles are a quasi-equilibrium configuration, as opposed to one constrained by diffusion, then it is possible to explain the absence of any systematic variation of filling rates with profile dimensions. The curvature is small for these profiles and any two-dimensional nucleation phenomena could be expected to proceed much as for planar surfaces. The nucleation of a two-dimensional

cavity on a ridge could be the rate limiting step during mass transfer to the channels. If this is true, then since dislocations are potential sites for the growth of these voids, the dislocation concentration could determine the mass transfer rate. A non-uniform dislocation concentration in the specimen could therefore result in varying profile decay rates.

The dislocations intersecting the surface of the wafer can be revealed using the method of Gilman and Johnston[43]. Following this method, the crystal was etched with CP-4 reagent for 90 s and rinsed in methanol and then ether. The resultant etch pits mark the location of dislocations intersecting the surface. An etched wafer surface is shown in Figure 13 with a 10/5 profile for reference. The micrographs indicate that the concentration of dislocations at the surface is not entirely uniform. Whether or not this non-uniformity is large enough to cause the rate fluctuations observed, some evidence is nevertheless present to support the above hypothesis.

The profile morphology depends upon the annealing atmosphere. In the studies already discussed, the initial annealing step was performed in vacuum (~10^{-7} Torr) and the subsequent anneals were performed in dry argon. However, two experiments were performed in which the initial anneal was performed in a closed chamber filled with air. Figure 14 shows micrographs of the specimen surface before this anneal, after this anneal and after a subsequent anneal at 770°C in argon for four hours.

It is clear from Figure 14 that the presence of air in the initial annealing step, while having no visible effect during the anneal, results in pronounced surface irregularity during subsequent anneals. Specifically, the surface appears to have formed many {100} steps along the channel walls and even in areas of the specimen

where no channels had been introduced. As mentioned earlier, Wang and co-workers have suggested that the H_2O or O_2 present in air can cause a lowering of the {100} surface tension, thereby causing these planes to be favored [7].

B. Particle Shape Studies

The as-received powder particles were roughly cubic, and the size range was about 1 to 5μm. A representative micrograph of the initial powder is shown in Figure 15.

The particle shape studies can be separated into two categories, namely 1) studies of isolated particles and small agglomerates, and 2) studies of bulk powder compacts.

1. Isolated particles and small agglomerates

Figure 16 shows particles isolated on the graphite substrate, before any heat treatment. The geometry is still cubic, but from the appearance of ledges and holes, it is apparent that some dissolution may have taken place during suspension in the ethanol/HCl solution.

Figure 17 shows the particles after heating at 680°C for 4 h in a ~10^{-6} Torr vacuum. After heat treatment, the large particles retained their cubic morphology, whether isolated or in small clusters. This leads to one of the following conclusions: a) for the temperatures used, the Gibbs-Wulff plot is not significantly altered from its zero-entropy form, or b) the cooling period following the treatment was slow enough to allow reconfigurations that do not represent the morphology at the annealing temperature. The cooling period lasted about three to five hours, so reconfigurations could be expected.

In order to determine which of the above conclusions is correct, experiments were performed using bulk powder compacts in which the specimen was quenched rapidly (again ≈5 s) to room temperature. The results of these experiments will be discussed in the next section.

Figure 18 shows particles which were heated at 680°C for 8 h in argon and then slow-cooled. In this experiment the particles are irregularly shaped and exhibit rounding. The rounding is presumably caused by adsorption of a species present in the argon. This conclusion is supported by evidence found in bulk compacts, which also will be discussed in the next section.

After the annealing treatment, many of the particles are surrounded by many smaller 'secondary' particles which were not initially present. It was suspected that these smaller particles are the result of precipitation of LiF from the suspending solution. The small particles are found primarily in the vicinity of the large particles where the solution dried last, and the concentration of lithium fluoride in solution was highest there.

To test this hypothesis, a suspending solution saturated with lithium fluoride, but not containing any large particles, was dried on a substrate. Figure 19 shows the substrate after drying, but before heat treatment. No large particles are present, but the dried liquid left behind a dendritic pattern over a large portion of the graphite. This pattern is presumably caused by the higher concentration of lithium fluoride in the saturated solution. Figure 20 shows the consequence of annealing the substrate with the dendritic pattern. The small "secondary" particles appeared and in some cases grew considerably during the treatment. The dendritic pattern disappeared, suggesting

that the small particles are formed by growth from a fine layer of lithium fluoride left behind after drying.

2. Bulk powder compacts

Typical morphologies corresponding to the various heat treatments of the bulk powder bed are shown in Figures 21, 22, and 23. Significant departure from the cubic geometry has occurred. Faces other than {100} type are visible, as in Figure 21, and some rounding of the corners and edges has occurred.

In those cases where the powder was annealed in vacuum at 680°C (see Figure 21) the average grain size increased from ~2 μm to ~3 μm. Many of the particles have a truncated cubic morphology, with {111} type faces forming at the corners. Also, while a small amount of rounding has occurred at the corners and edges, the particles are still highly facetted. Even where particles meet, the neck area is not rounded at the magnification used in most cases.

When the annealing temperature was raised to 760°C, much more rounding occurred, as can be seen in Figure 22. More interparticle neck growth is observed as sintering takes place as well. One particular feature of the higher temperature anneal that is different from the lower temperature anneal is the appearance of terraces. Once again, this feature may be caused by a slow cooling period following the anneal, during which reconfigurations occur that produce growth terraces. To determine if the terraces are the result of slow cooling, a 760°C anneal was performed followed by a 5 s quench to room temperature. The resulting microstructure can be seen in Figure 23. The degree of rounding is similar to the slowly cooled microstructure, but most of the

terraces are absent, indicating that the terraces formed during slow cooling as a result of reconfiguration. Thus, Figure 23 more accurately represents the microstructure prevalent at 760°C than Figure 22.

Powder bed anneals were also performed in which the furnace chamber was back-filled with one atmosphere of 99.98% pure dry argon. As can be seen in Figure 24 significant rounding of the particles occurred even at 680°C. Previous experiments showed little rounding at this temperature. This extensive rounding could be a result of the surface adsorption of an impurity species in the argon. Impurity adsorption will occur spontaneously only if it results in a lowering of the surface tension. As a result, adsorption could cause a decrease in the surface tension anisotropy, since the anisotropy of the lithium fluoride/impurity layer interface may be less marked than the anisotropy of the lithium fluoride/vapor interface. While results of experiments on single crystal lithium fluoride surfaces indicate that species in air can preferentially adsorb during high temperature anneals, the effect of these impurities was to promote formation of {100} surfaces [7]. In addition, studies performed on cleaved {100} LiF surfaces indicate that H_2O adsorbs on these surfaces only below 200 K [44]. Although these results may not strictly apply to powder beds, they do make the effect of impurities seem unlikely as a cause of rounding.

While impurity adsorption is a possible mechanism for rounding, it is also possible that the rounding is caused by an entropy-induced smoothing of the Gibbs-Wulff plot. However, smoothing of the γ-plot would not be expected in the powder bed any more than in the experiments with individual particles since the annealing temperatures were identical.

Since extensive rounding has occurred during the 760°C anneal, the surface tension is presumably more isotropic at this temperature than at 680°C. One possible reason for this is the occurrence of surface melting of the individual particles, as discussed in the previous section. For a liquid LiF layer to completely wet a LiF crystal plane *i* requires that the liquid/solid interfacial energy be less than the difference between γ_{sv_i}, the solid/vapor surface tension of the *i*th surface, and γ_{lv_i}, the liquid/vapor surface tension above the *i*th surface. That is

$$\gamma_{ls_i} < \gamma_{sv_i} - \gamma_{sv_i} \tag{4}$$

In Equation (4), γ_{lv_i} is independent of *i* and γ_{sl_i} is likely to vary more or less in direct proportion to γ_{sv_i} because ions of the liquid at the solid/liquid interface can occupy roughly the positions that they would if the solid structure continued into the liquid.

Another possible explanation for rounding is given by Brailsford and Gjostein[45], and involves the following argument. Given two particles whose equilibrium shapes are faceted, when these particles contact each other the driving force for coalescence can cause large diffusional fluxes to the neck. This fast transport of material involves the atoms on the faceted surfaces and can therefore destroy the faceted shape unless the facets can quickly reform. Once the two particles have coalesced to the point that the neck is eliminated, the diffusional fluxes are greatly reduced and the remaining particle may again assume a faceted equilibrium shape. Brailsford and Gjostein have also presented experimental data for gold crystallites that supports this argument.

By generalizing to a powder compact, the above argument provides another possible explanation for the rounding of lithium fluoride particles. In contrast to the

explanations provided earlier, this argument makes no assumption about the relative surface energy anisotropy at different temperatures. However, the relative rates of surface diffusion and facet reformation are not likely to vary dramatically over a modest temperature range without a change in the anisotropy. Therefore this argument does not seem to lend support to the experimental observation that the compact microstructure changes from faceted at lower temperatures to rounded at higher temperature unless a change in anisotropy is incorporated. Also, since the relative rates of surface diffusion and facet reformation for lithium fluoride particles in the micron size range are not known to the author, it is difficult to test this argument as a mechanism for rounding at high temperature.

IV. Summary

A reversible rounded/facetted transition has been observed on lithium fluoride surfaces, both for periodic profiles on single crystals and for small particles.

For initially facetted profiles, the profile amplitude was observed to round significantly and decay with time at temperatures near 93% of the bulk melting point. When these rounded profiles were slowly cooled they refacetted over a temperature range below 89% of the melting point if the profiles were shallow (~0.5 μm), but when deeper (~1.0 μm) the refaceting occurred only if the specimen was held at a lower temperature (90% of the melting point) and then slowly cooled. The transition temperature range has not yet been determined, but a determination of the broadness of the range could indicate the operative mechanism in the transition.

The rate of decay of the rounded profiles was dependent on the profile dimensions, but the scatter in the data made quantitative analysis of the filling unfeasible. Removal of material from the ridges was hypothetically proposed to be the rate limiting step in the process, and under this hypothesis the erratic decay rate behavior was attributed to a non-uniform dislocation concentration.

It was also observed that the morphology exhibited was dependent on atmosphere. When annealed in air, irregularities appeared which increased the surface area. These irregularities did not appear when the profiles were annealed in argon and in vacuum. A possible explanation for the appearance of the irregularities is adsorption of a species, such as O_2 or H_2O.

Initially facetted lithium fluoride particles (~5.0 μm) were observed to remain facetted when isolated on a graphite chip and heated to 85% of the melting point, but

rounded at the same temperature when in bulk powder form. Bulk powder heated to 93% of the melting point exhibited further rounding, but if slowly cooled to room temperature the particles developed facetted ledges, giving confirmation of the rounded/facetted transition.

Appendix

Atomic emission spectroscopy was performed[m] on both the single crystal wafer[n] and the powder[o]. The technique resulted in qualitative and semi-quantitative information about the impurity content of the specimens. A simultaneous scan of 45 elements was performed, with the sensitivity of detection depending on the individual element. All data below is given in parts per million (ppm). The symbol N indicates that the element was not detected for the given sensitivity limit.

Element	Limit	Wafer	Powder	Element	Limit	Wafer	Powder
Antimony	5	N	N	Mercury	10	N	N
Aluminum	10	N	100-300	Molybdenum	1	N	N
Arsenic	100	N	N	Niobium	10	N	N
Barium	100	N	N	Nickel	1	N	N
Beryllium	0.5	N	N	Palladium	1	N	N
Bismuth	1	N	N	Phosphorus	500	N	N
Boron	5	N	N	Platinum	10	N	N
Cadmium	10	N	N	Rhodium	5	N	N
Calcium	50	N	N	Ruthenium	5	N	N
Chromium	5	N	N	Scandium	100	N	N
Cobalt	5	N	N	Silicon	10	N	N
Copper	5	N	N	Silver	0.5	N	N
Gallium	5	N	N	Sodium	1000	N	N
Germanium	5	N	N	Tantalum	10	N	N
Gold	5	N	N	Thallium	5	N	N
Hafnium	100	N	N	Tin	1	N	10-30
Indium	1	N	N	Titanium	5	N	N
Iridium	50	N	N	Tungsten	10	N	N
Iron	1	N	N	Vanadium	1	N	N
Lanthanum	100	N	N	Yttrium	100	N	N
Lead	0.5	N	N	Zinc	50	N	N
Magnesium	0.5	N	N	Zirconium	10	N	N
Manganese	0.5	N	N				

[m]Spectra Co., San Diego, California

[n]Englehard Company, Solon, Ohio

[o]Johnson Matthey, Materials Technology, England.

Tables

Milling Parameter	Value
Accelerating Voltage	900 V
Cathode Current	19 mA
Arc Current	1 A
Arc Voltage	30 - 60 V
Magnetic Coil Current	0.8 A
Suppressor Voltage	250 V

Table 1. Milling parameters for Veeco argon ion mill

Channel/Ridge width (μm)	Initial Depth (μm)		Annealed Depth (μm)		Depth Change (μm)	
	$\bar{d}_1$	σ_1	$\bar{d}_2$	σ_2	$\bar{d}_1 - \bar{d}_2$	$\sigma_1 + \sigma_2$
5/5(4.954)	0.787	0.107	0.227	0.084	0.510	0.191
5/10(9.659)	0.868	0.088	0.649	0.134	0.219	0.222
5(6.441)/25	0.985	0.088	0.517	0.187	0.468	0.275
10/5(5.056)	0.704	0.067	0.353	0.009	0.351	0.076
10/10(9.756)	0.782	0.035	0.571	0.103	0.211	0.138
10(10.897)/25	0.935	0.029	--	--	--	--
10(11.024)/100	1.068	0.058	0.500	--	0.568	--
25/5(5.650)	0.640	0.096	0.356	0.048	0.284	0.144
25/10(10.135)	0.576	0.068	0.465	0.089	0.111	0.157
25/25	0.636	0.072	0.632	0.049	0.004	0.121

Table 2. Depth measurements on profiles from a specimen milled for 12 min. Initial facetted profiles result from an anneal at 550°C for 15 h, 10^{-7} Torr, and have mean depths $\bar{d}_1$ and standard deviations σ_1. Profiles after an anneal in argon at 770°C for 4 h are rounded and have mean depths $\bar{d}_2$ and standard deviations σ_2. Numbers in parentheses indicate actual width measurements for comparison with those designed into the mask, and also indicate whether the profile measurements were taken on the spacing between channels (parentheses follow second number) or on the channel (parentheses follow first number).

Channel/Ridge width (μm)	Initial Area (μm^2)		Annealed Area (μm^2)		Area Change (μm^2)	
	$\bar{A}_1$	σ_1	$\bar{A}_2$	σ_2	$\bar{A}_1 - \bar{A}_2$	$\sigma_1 + \sigma_2$
5/5(4.954)	3.227	0.217	0.840	0.206	2.387	0.423
5/10(9.659)	6.849	0.503	4.389	0.717	2.460	1.220
5(6.441)/25	5.186	0.506	2.560	1.226	2.626	1.732
10/5(5.056)	2.821	0.123	1.069	0.050	1.752	0.173
10/10(9.756)	5.714	0.588	3.647	0.873	2.067	1.461
10(10.897)/25	--	--	--	--	--	--
10(11.024)/100	10.079	0.443	4.105	0.316	5.974	0.759
25/5(5.650)	2.736	0.462	1.056	0.124	1.680	0.586
25/10(10.135)	4.840	0.495	2.692	1.209	2.148	1.704
25/25	--	--	--	--	--	--

Table 3. Cross-sectional area measurements on profiles for the same specimens described in Table 2. Profiles of specimens annealed in argon at 770°C for 4 h have mean areas $\bar{A}_2$ and standard deviations σ_2. Numbers in parentheses indicate actual width measurements for comparison with those designed into the mask, and also indicate whether the profile measurements were taken on the spacing between channels (parentheses follow second number) or on the channel (parentheses follow first number).

Channel/Ridge width (μm)	Initial Depth (μm)		Annealed Depth (μm)		Depth Change (μm)	
	$\bar{d}_1$	σ_1	$\bar{d}_2$	σ_2	$\bar{d}_1 - \bar{d}_2$	$\sigma_1 + \sigma_2$
5/5(4.954)	0.787	0.107	--	--	--	--
5/10(9.659)	0.868	0.088	--	--	--	--
5(6.441)/25	0.985	0.088	--	--	--	--
10/5(5.056)	0.704	0.067	0.529	0.111	0.175	0.178
10/10(9.756)	0.782	0.035	0.735	0.083	0.047	0.118
10(10.897)/25	0.935	0.029	--	--	--	--
10(11.024)/100	1.068	0.058	0.547	0.078	0.388	0.107
25/5(5.650)	0.640	0.096	0.345	0.053	0.295	0.149
25/10(10.135)	0.576	0.068	--	--	--	--
25/25	0.636	0.072	--	--	--	--

Table 4. Depth measurements on profiles from specimens milled for 12 min. Initial profiles were annealed at 550°C for 15 h, 10^{-7} Torr, and have mean depths $\bar{d}_1$ and standard deviations σ_1. Specimen was annealed in argon at 770°C for 4 h, quenched, reannealed in argon at 725°C for 4 h and quenched again. The resulting rounded profiles have mean depths $\bar{d}_2$ and standard deviations σ_2. Numbers in parentheses indicate actual width measurements for comparison with those designed into the mask, and also indicate whether the profile measurements were taken on the spacing between channels (parentheses follow second number) or on the channel (parentheses follow first number).

Channel/Ridge width (μm)	Initial Area (μm^2)		Annealed Area (μm^2)		Area Change (μm^2)	
	$\bar{A}_1$	σ_1	$\bar{A}_2$	σ_2	$\bar{A}_1 - \bar{A}_2$	$\sigma_1 + \sigma_2$
5/5(4.954)	3.227	0.217	--	--	--	--
5/10(9.659)	6.849	0.503	--	--	--	--
5(6.441)/25	5.186	0.506	--	--	--	--
10/5(5.056)	2.821	0.123	1.427	0.121	1.398	0.244
10/10(9.756)	5.714	0.588	4.471	0.081	1.243	0.669
10(10.897)/25	--	--	--	--	--	--
10(11.024)/100	10.079	0.443	2.486	0.607	5.784	1.164
25/5(5.650)	2.736	0.462	0.970	0.118	1.766	0.580
25/10(10.135)	4.840	0.495	--	--	--	--
25/25	--	--	--	--	--	--

Table 5. Cross-sectional area measurements on profiles for the same specimens described in Table 4. Specimen was annealed in argon at 770°C for 4 h, quenched, reannealed in argon at 725°C for 4 h and quenched again. The resulting rounded profiles have mean areas $\bar{A}_2$ and standard deviations σ_2. Numbers in parentheses indicate actual width measurements for comparison with those designed into the mask, and also indicate whether the profile measurements were taken on the spacing between channels (parentheses follow second number) or on the channel (parentheses follow first number).

Channel/Ridge width (μm)	Initial Depth (μm)		Annealed Depth (μm)		Depth Change (μm)	
	$\bar{d}_1$	σ_1	$\bar{d}_2$	σ_2	$\bar{d}_1 - \bar{d}_2$	$\sigma_1 + \sigma_2$
5/5(2.532)	1.022	0.099	0.305	0.071	0.717	0.170
5/10	1.180	0.088	0.680	0.074	0.500	0.162
5/25	1.516	0.042	0.910	0.070	0.606	0.112
10/5(2.047)	1.076	0.153	0.325	0.036	0.751	0.189
10/10	1.250	0.173	0.588	0.104	0.662	0.277
10/25	1.386	0.090	0.912	0.080	0.474	0.170
10/100	1.535	0.074	1.038	0.215	0.497	0.289
25/5(3.054)	0.935	0.051	0.368	0.030	0.567	0.081
25/10	1.031	0.108	0.628	0.060	0.403	0.168
25/25	1.164	0.155	0.956	0.149	0.208	0.304

Table 6. Depth measurements on profiles from a specimen milled for 20 min. Initial profiles were annealed at 550°C for 15 h, 10^{-7} Torr, and have mean depths $\bar{d}_1$ and standard deviations σ_1. Specimen was annealed in argon at 770°C for 8 h and cooled slowly to room temperature. The resulting profiles have mean depths $\bar{d}_2$ and standard deviations σ_2. Numbers in parentheses indicate actual width measurements for comparison with those designed into the mask, and also indicate whether the profile measurements were taken on the spacing between channels (parentheses follow second number) or on the channel (parentheses follow first number).

Channel/Ridge width (μm)	Depth Before (μm)		Depth After (μm)		Depth Change (μm)	
	$\bar{d}_1$	σ_1	$\bar{d}_2$	σ_2	$\bar{d}_1 - \bar{d}_2$	$\sigma_1 + \sigma_2$
5/10	1.474	0.149	0.880	0.174	0.594	0.323
5/25	1.398	0.444	0.982	0.042	0.416	0.486
10/10	1.188	0.092	0.715	0.043	0.473	0.135
10/25	1.232	0.013	1.102	0.042	0.130	0.055
10/100	1.702	0.107	1.449	--	0.253	--
25/5	0.932	0.235	0.783	0.149	0.149	0.384

Table 7. Depth measurements on profiles from a specimen milled for 20 min. Specimen was annealed at 550°C for 15 h, 10^{-7} Torr, then annealed in argon at 770°C for 8 h. The resulting rounded profiles have mean depths $\bar{d}_1$ and standard deviations σ_1. The specimen was then annealed in argon at 730°C for 16 h and cooled slowly to room temperature. The resulting facetted profiles have mean depths $\bar{d}_2$ and standard deviations σ_2. Numbers in parentheses indicate actual width measurements for comparison with those designed into the mask, and also indicate whether the profile measurements were taken on the spacing between channels (parentheses follow second number) or on the channel (parentheses follow first number).

Figures

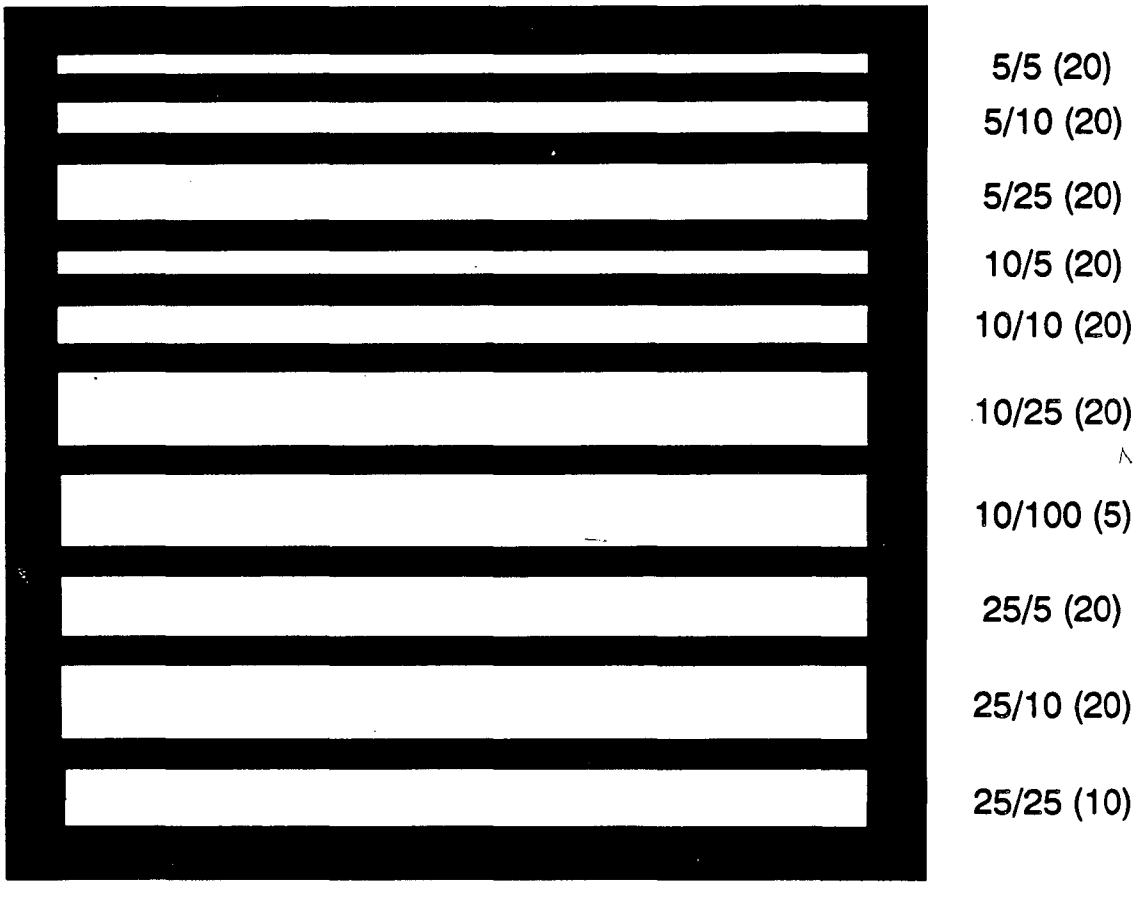

Figure 1. Photolithography mask layout. First number is channel width in microns, second number is distance between channels in microns, and third number is the number of channels in the profile. Actual size of exposed pattern is 6 mm x 6 mm, with a 150 micron separation between each profile.

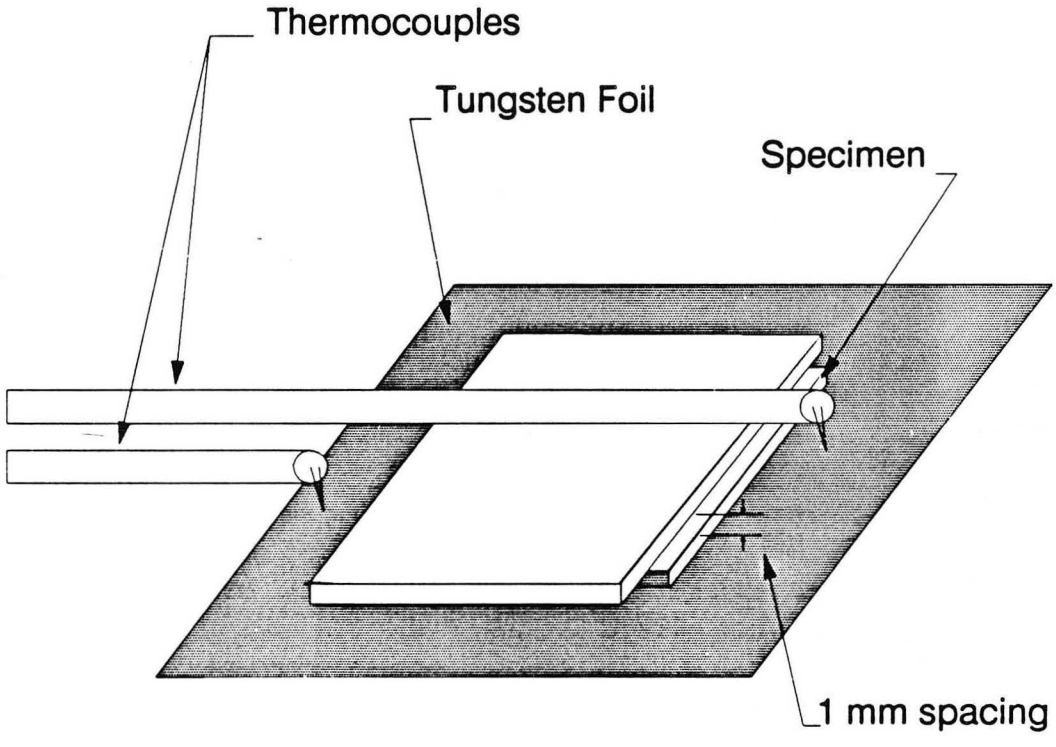

Figure 2. Experimental setup for channel heat treatments

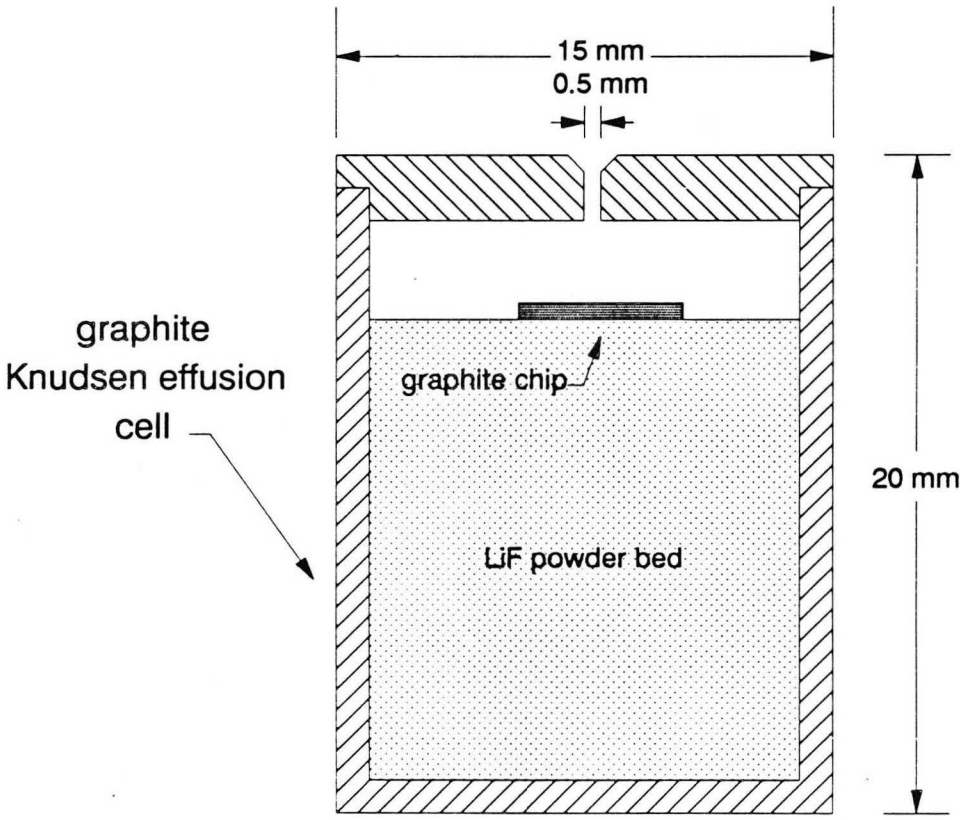

Figure 3. Experimental apparatus for particle shape experiments
(Cross-sectional view)

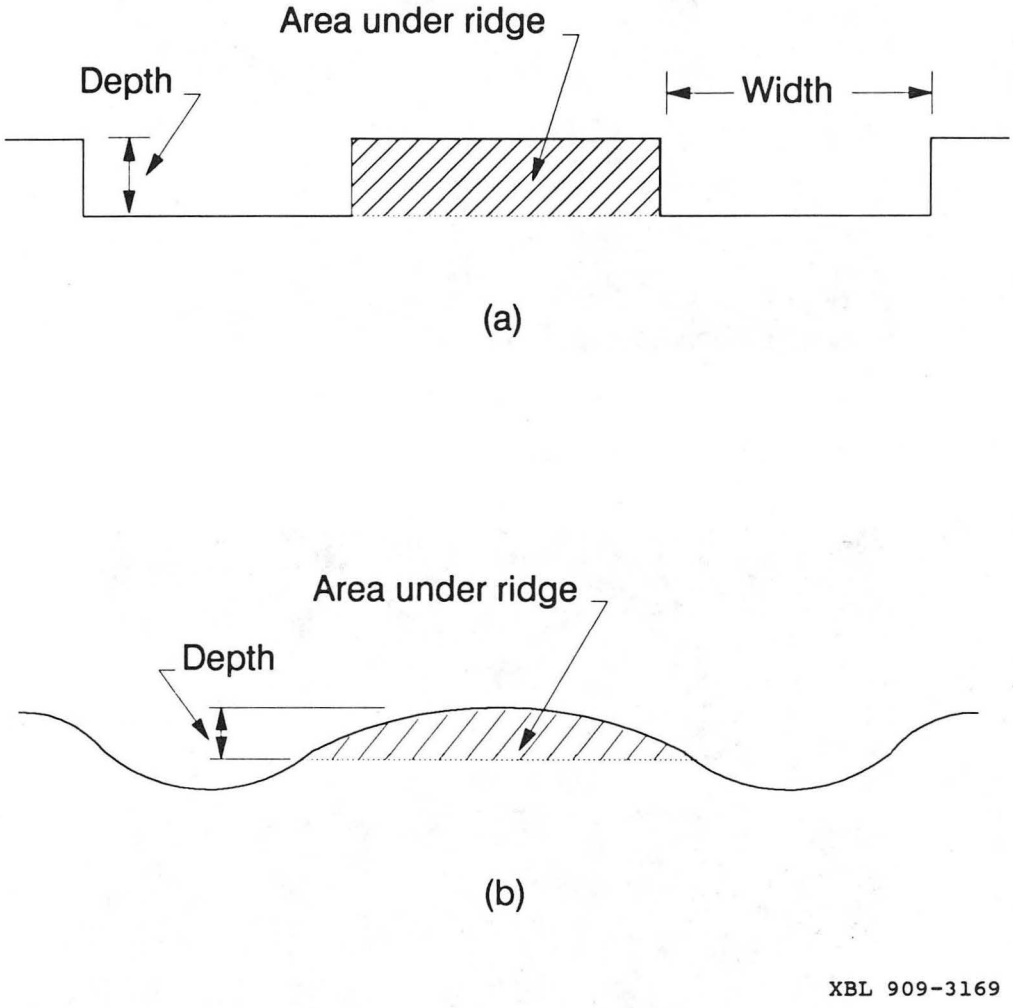

Figure 4. Dimensions of interest for (a) initial and faceted profiles, and (b) rounded profiles.

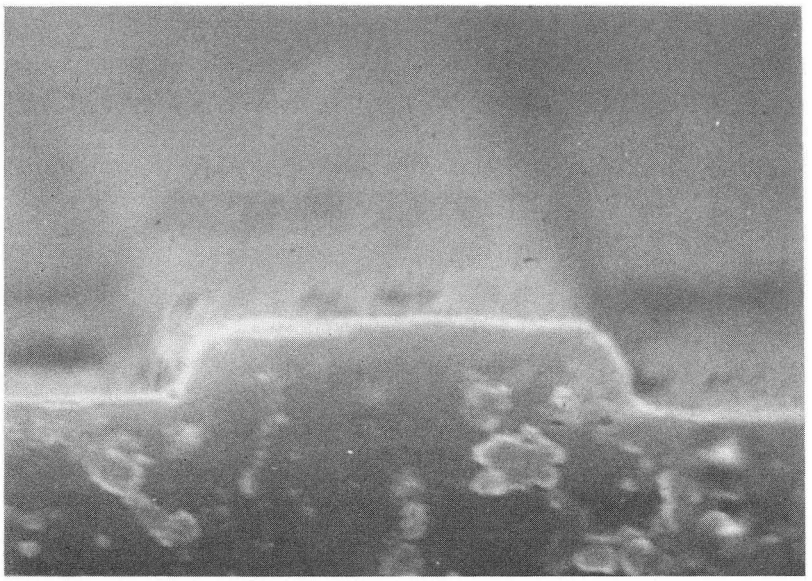

(a) —— 0.741 μm

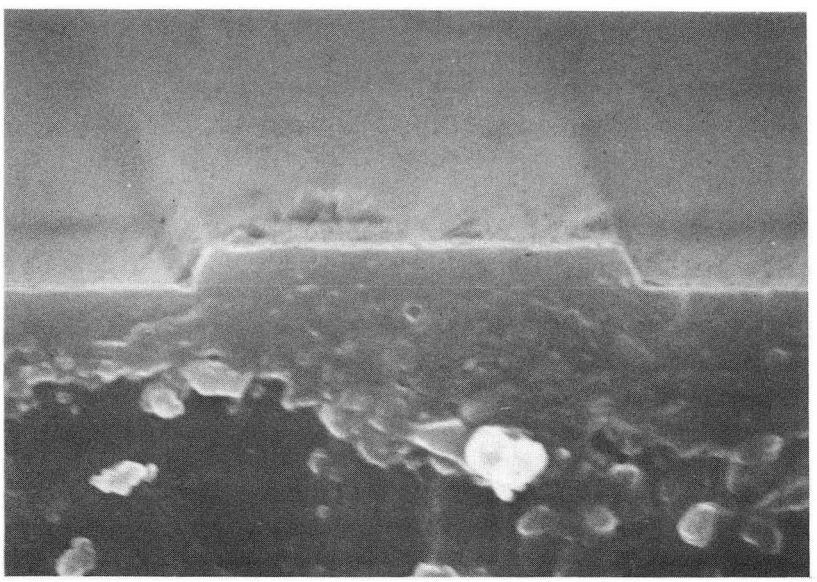

XBB 909-7702

(b) —— 1.47 μm

Figure 5. Initial profiles (a) 5/5 and (b) 5/10, using a 12 min milling time.

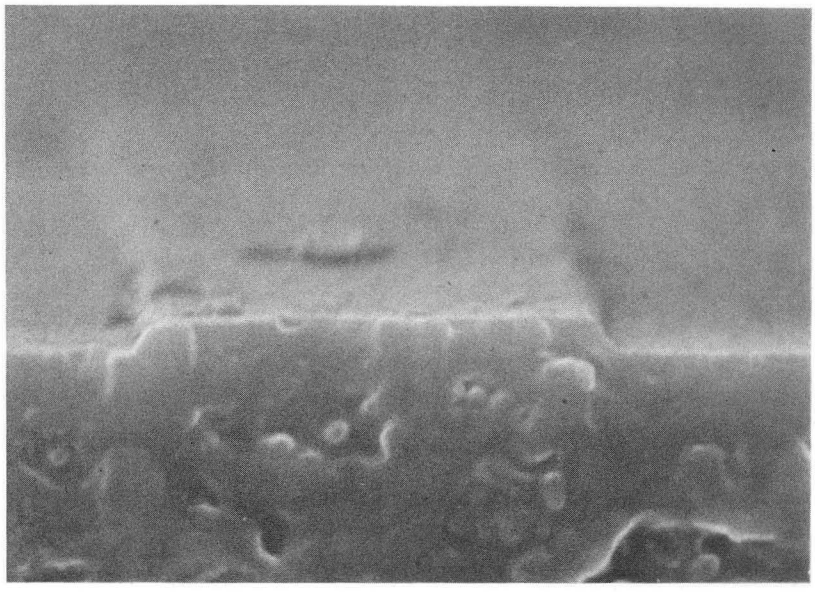

(c) —— 1.47 μm

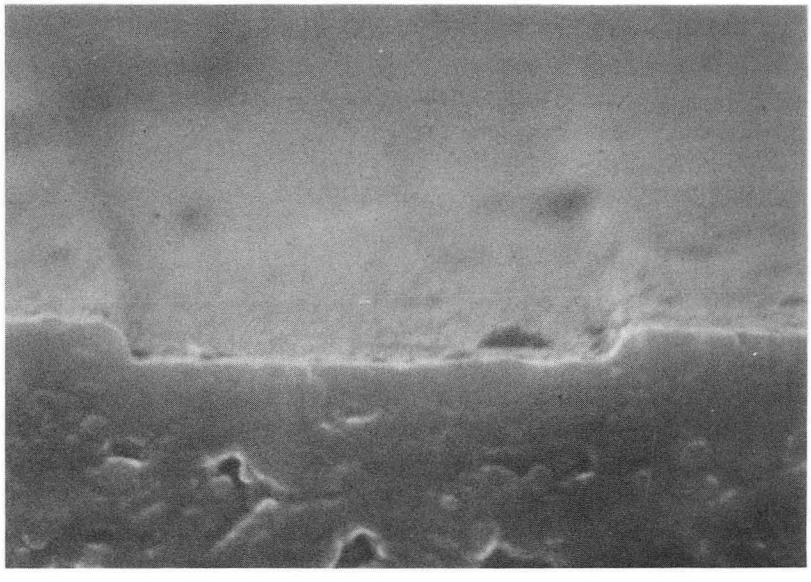

XBB 909-7703

(d) —— 1.47 μm

Figure 5 (cont'd). Initial profiles (c) 10/10 and (d) 10/25, using a 12 min milling time.

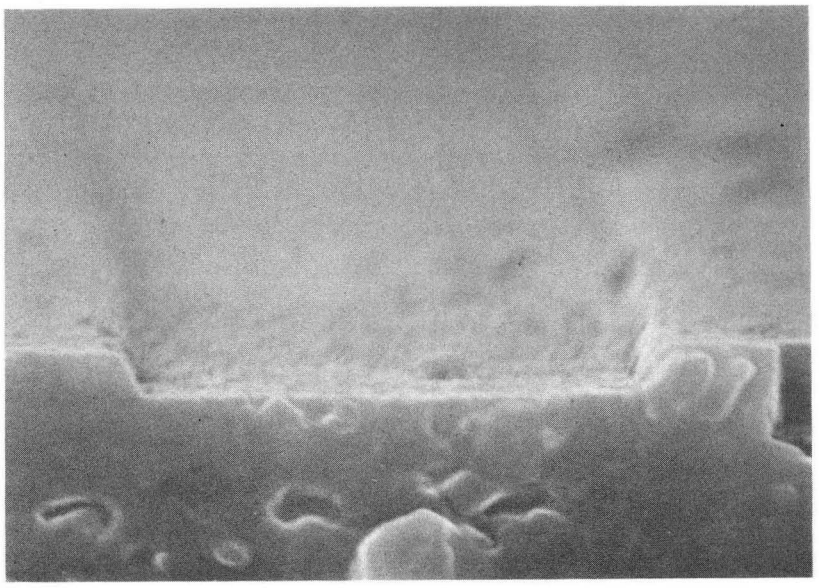

(e) —— 1.47 μm

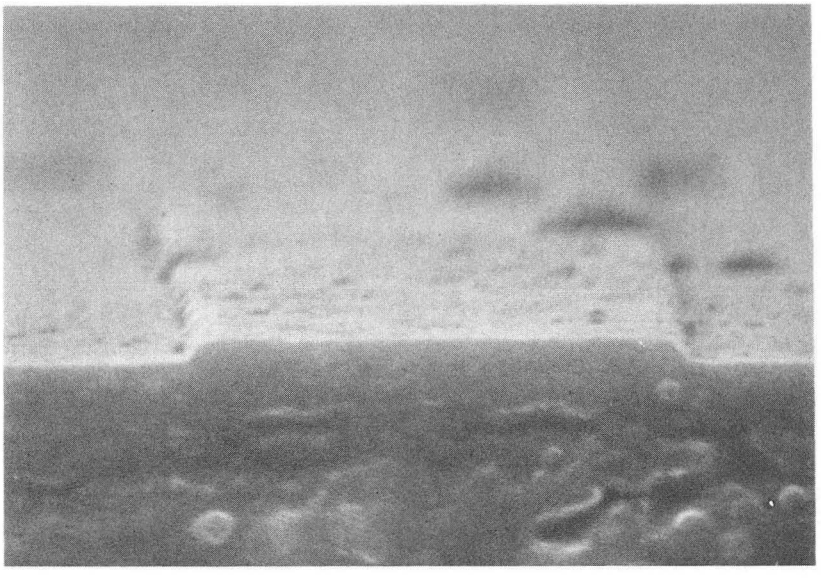

XBB 909-7704

(f) —— 1.47 μm

Figure 5 (cont'd). Initial profiles (e) 10/100 and (f) 25/5, using a 12 min milling time.

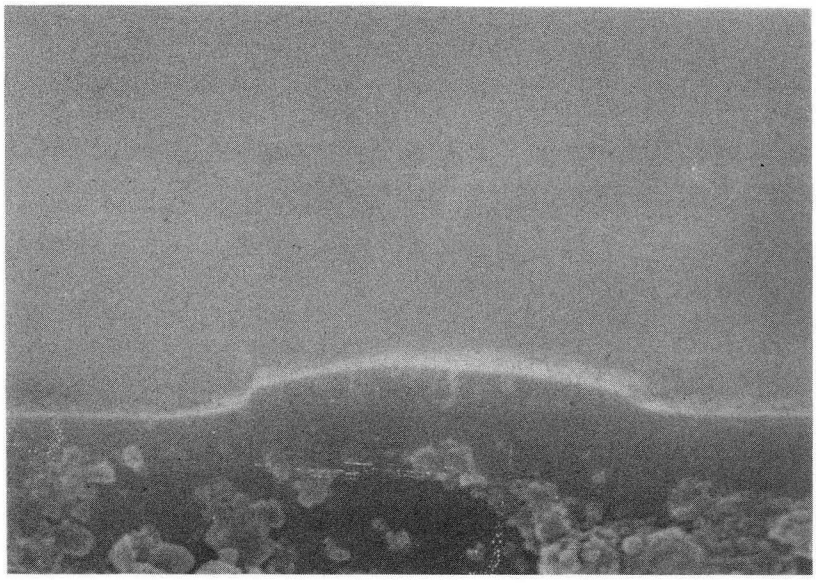

(a) —— 0.741 μm

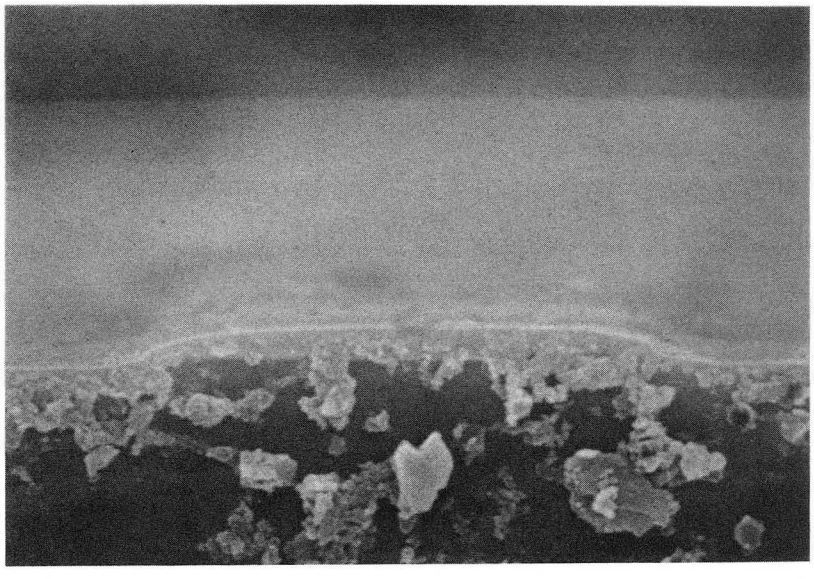

XBB 909-7705

(b) —— 1.23 μm

Figure 6. Profiles of specimens annealed at 770°C for 4 h in argon and then quenched to room temperature. Profiles shown are (a) 5/5 and (b) 5/10.

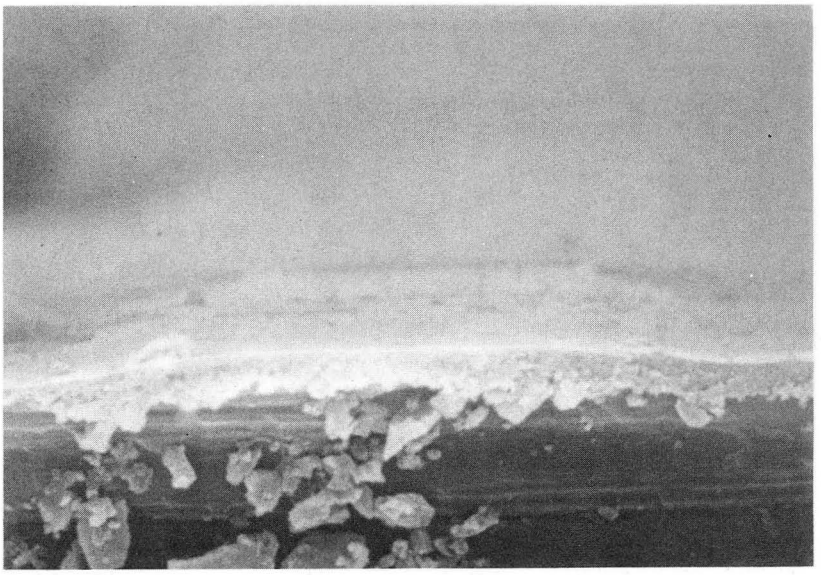

(c) —— 1.23 μm

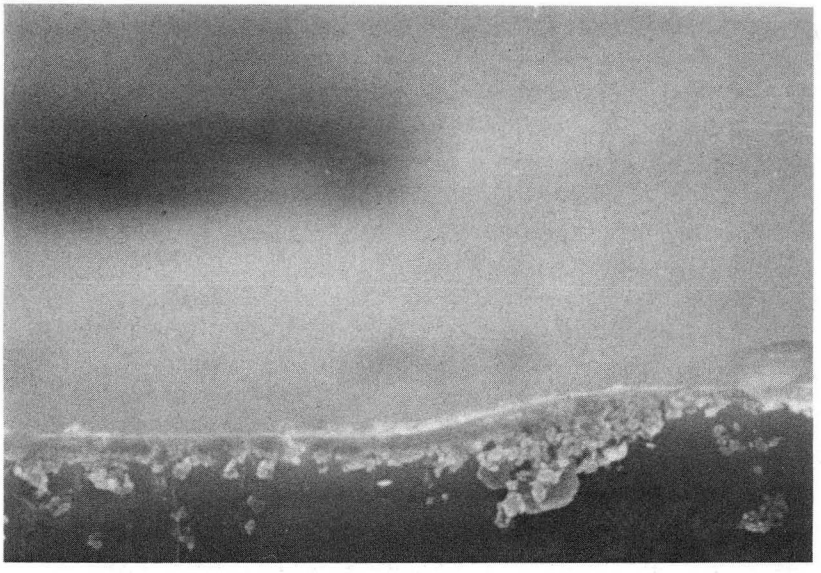

XBB 909-7706

(d) —— 1.23 μm

Figure 6 (cont'd). Profiles of specimens annealed at 770°C for 4 h in argon and then quenched to room temperature. Profiles shown are (c) 10/10 (d) 10/25.

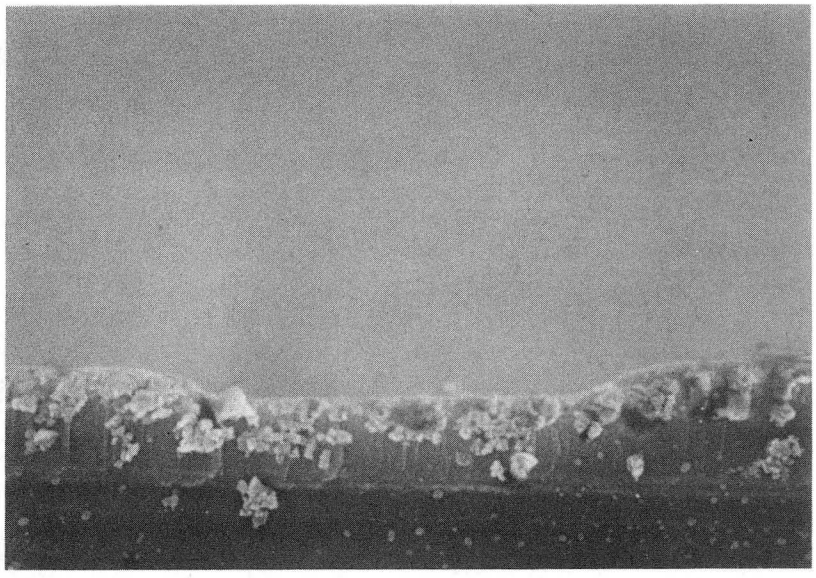

(e) —— 1.82 μm

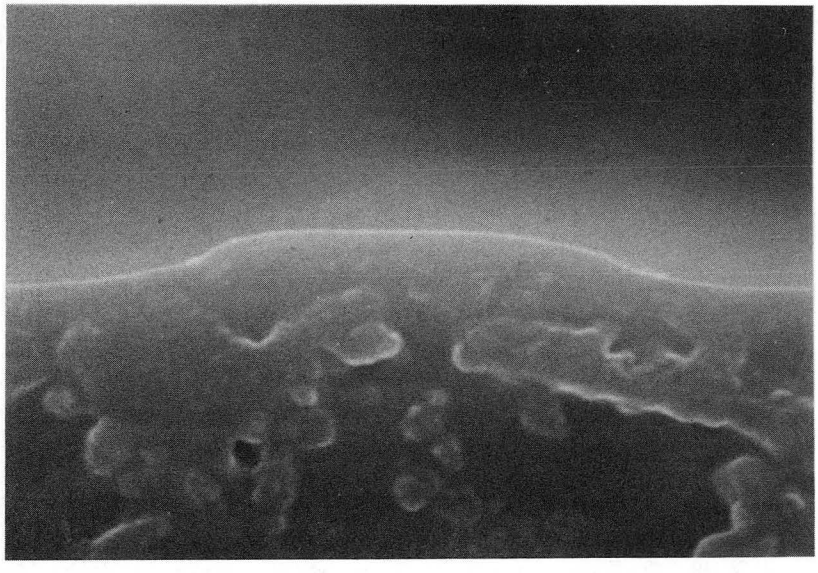

XBB 909-7707

(f) —— 0.730 μm

Figure 6 (cont'd). Profiles of specimens annealed at 770°C for 4 h in argon and then quenched to room temperature. Profiles shown are (e) 10/100 and (f) 25/5.

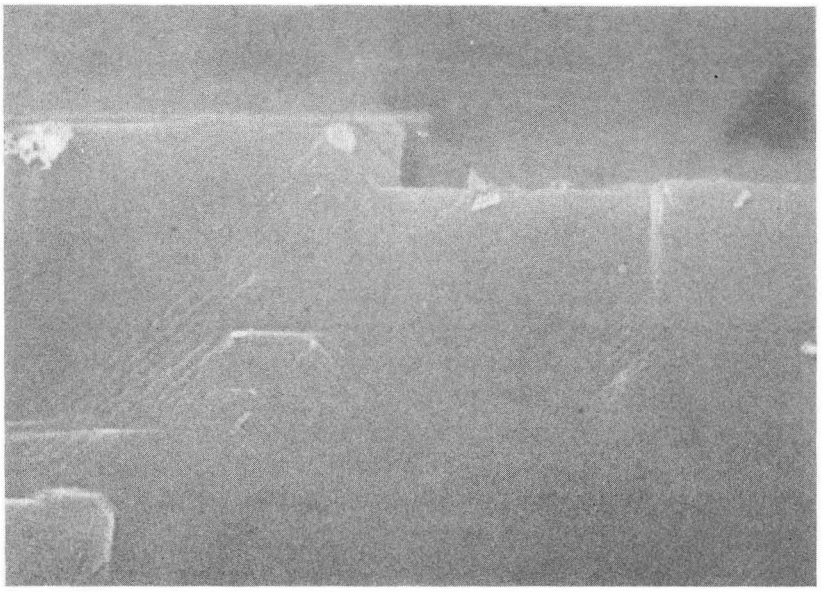

(a) —— 0.813 μm

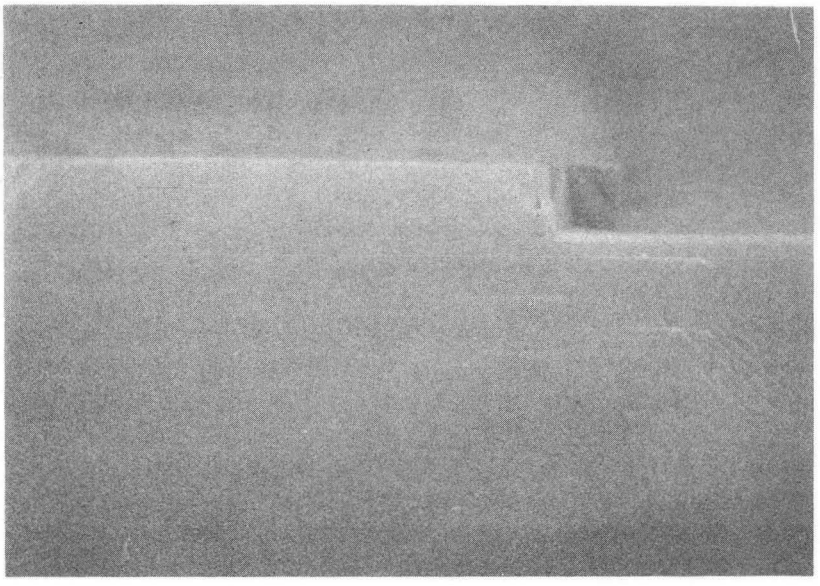

XBB 909-7708

(b) —— 0.813 μm

Figure 7. Profiles of specimens annealed at 770°C for 4 h in argon and slowly cooled to room temperature.

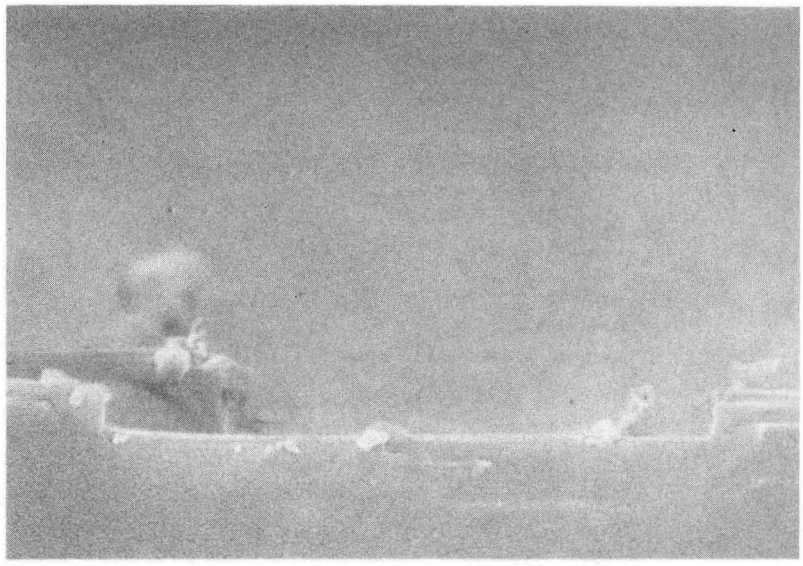

(c) —— 0.813 μm

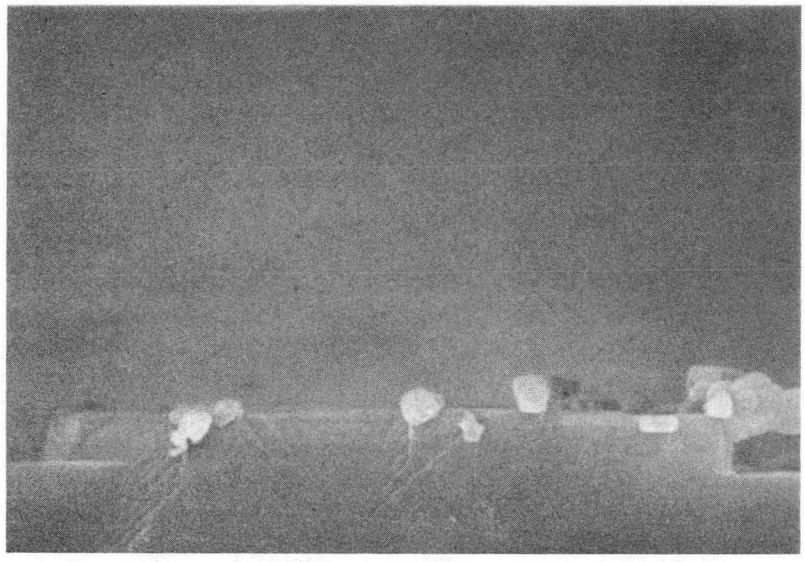

XBB 909-7709

(d) —— 0.813 μm

Figure 7 (cont'd). Profiles of specimens annealed at 770°C for 4 h in argon and slowly cooled to room temperature.

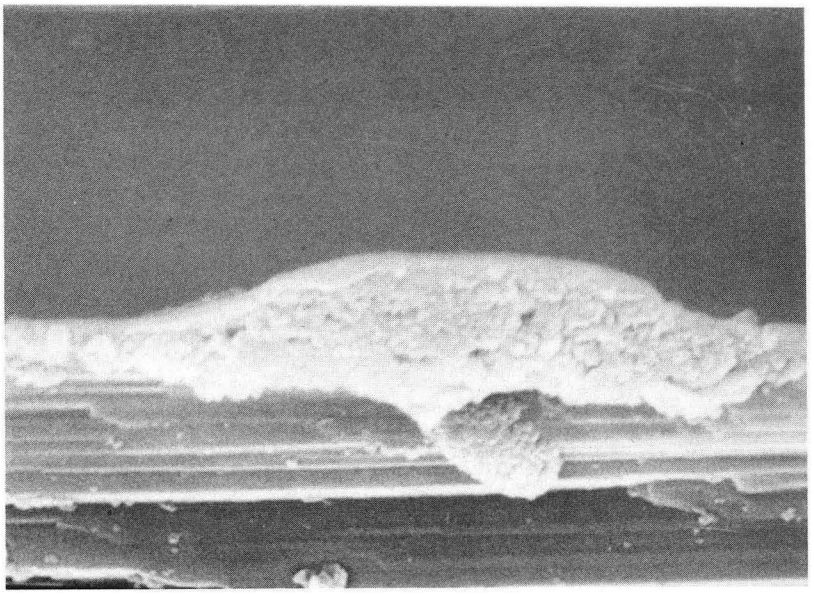

(a) —— 0.741 μm

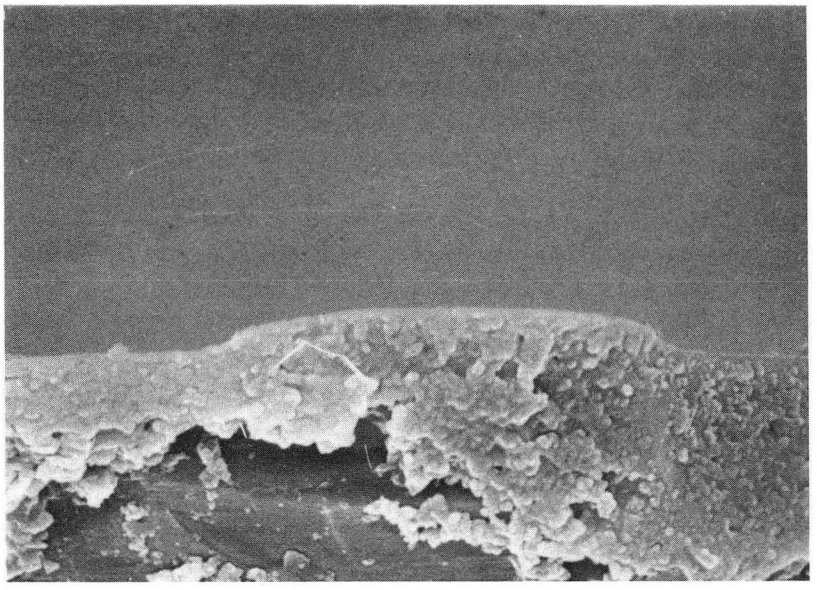

XBB 909-7710

(b) —— 1.47 μm

Figure 8. Profiles of specimens annealed at 770°C for 4 h in argon, quenched, then reannealed at 725°C for 4 h in argon and quenched. Profiles shown are (a) 10/5 and (b) 10/10.

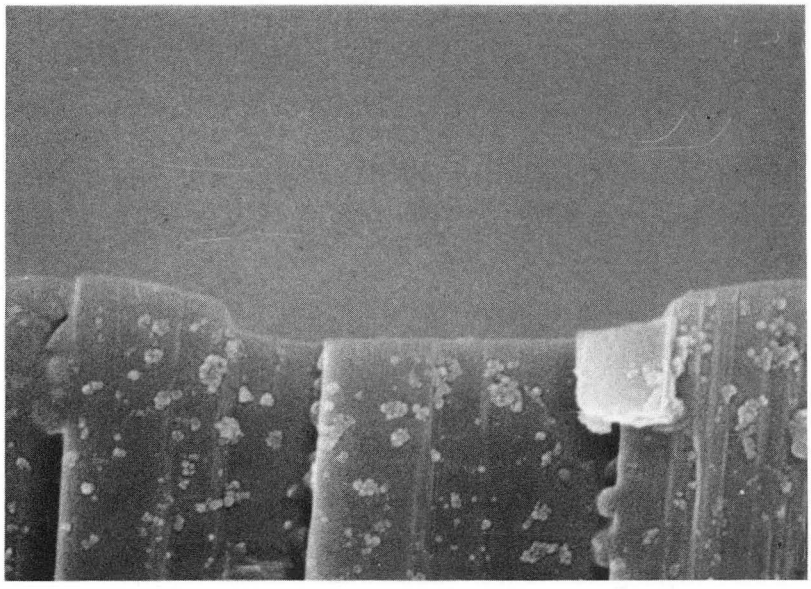

(c) —— 0.980 μm

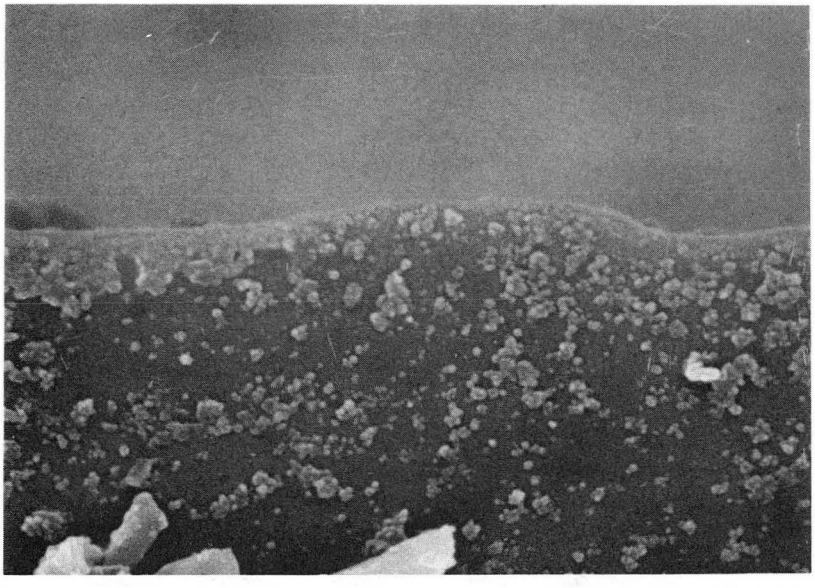

XBB 909-7711

(d) —— 0.980 μm

Figure 8 (cont'd). Profiles of specimens annealed at 770°C for 4 h in argon, quenched, then reannealed at 725°C for 4 h in argon and quenched. Profiles shown are (c) 10/25 and (d) 25/5.

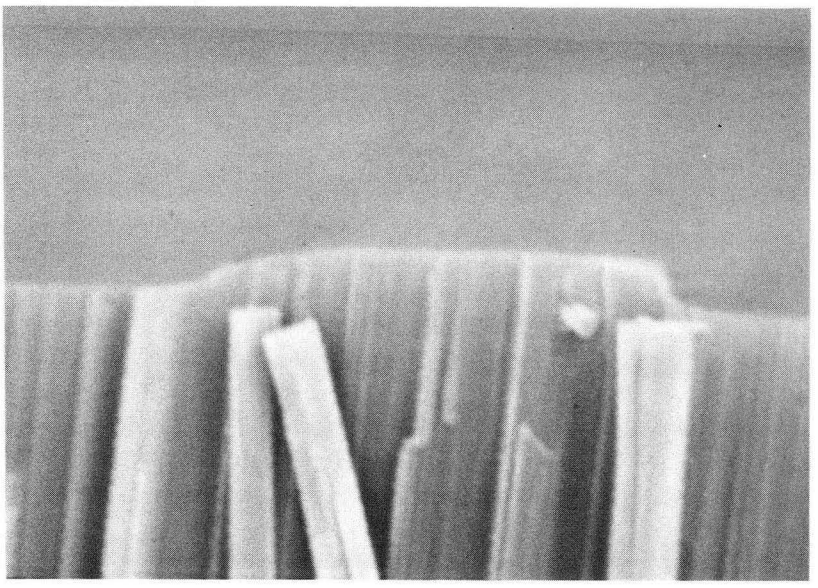

(a) —— 0.741 μm

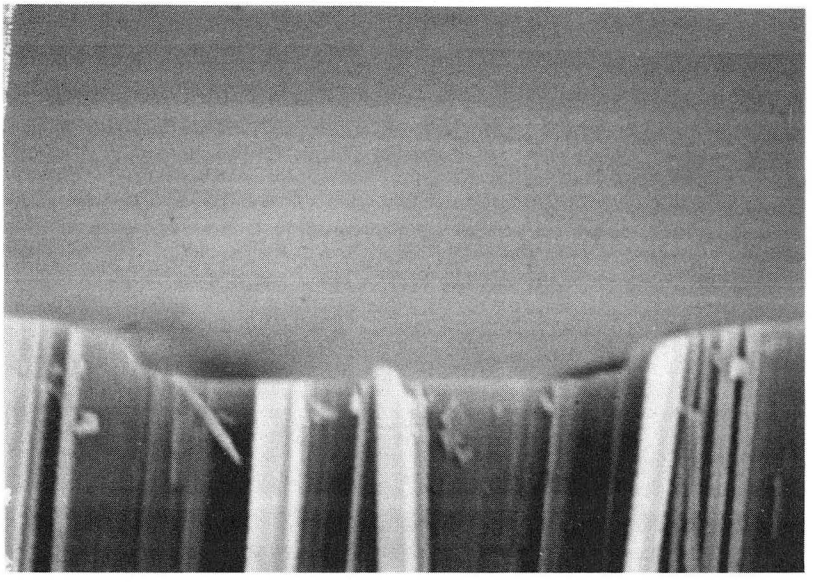

XBB 909-7712

(b) —— 0.980 μm

Figure 9. Profiles of specimens annealed at 770°C for 4 h in argon, cooled to 725°C, and then rapidly quenched to room temperature. Profiles shown are (a) 5/5 and (b) 5/25.

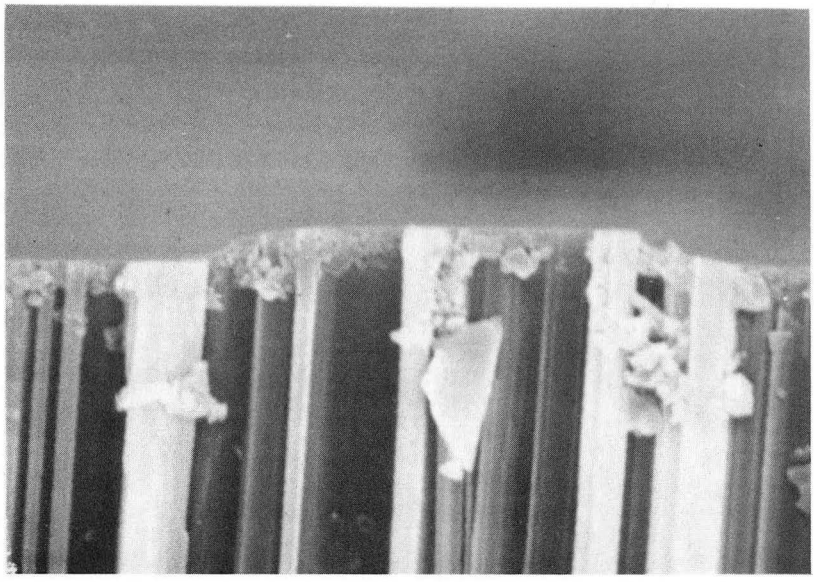

(c) —— 1.47 μm

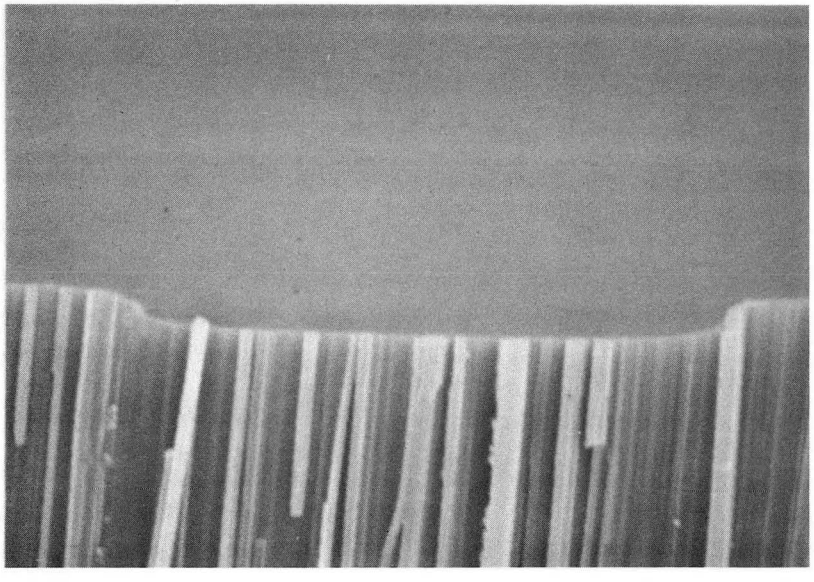

XBB 909-7713

(d) —— 1.47 μm

Figure 9 (cont'd). Profiles of specimens annealed at 770°C for 4 h in argon, cooled to 725°C, and then rapidly quenched to room temperature. Profiles shown are (c) 10/10 and (d) 10/25.

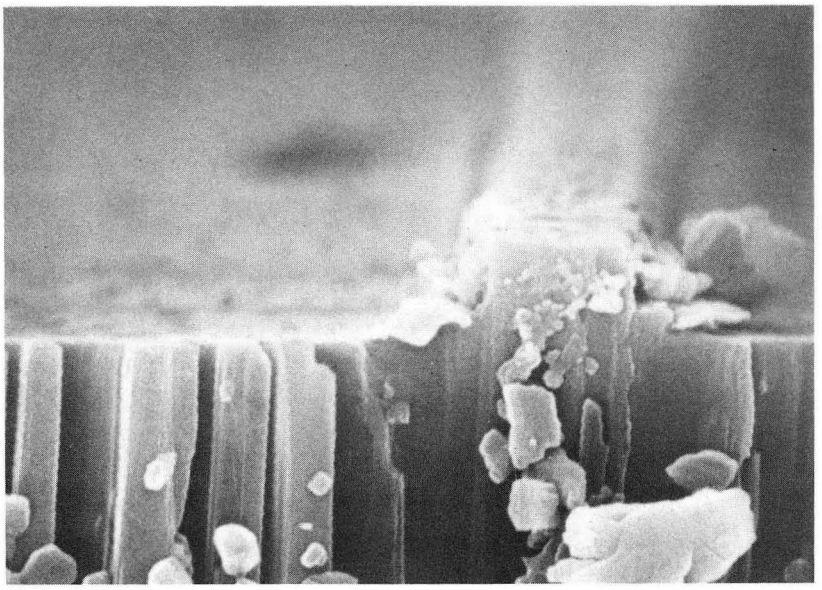

(a) —— 0.741 μm

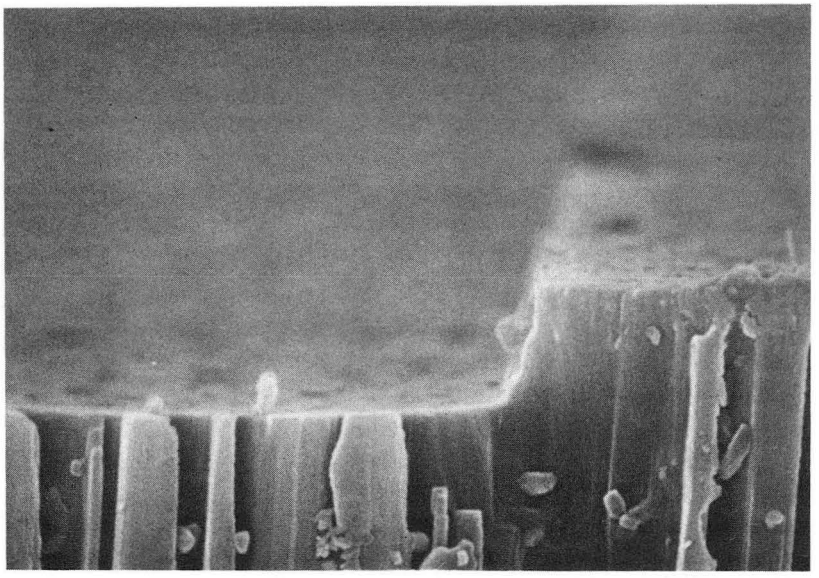

XBB 909-7714

(b) —— 0.741 μm

Figure 10. Initial profiles (a) 5/5 and (b) 5/10, using a 20 min milling time.

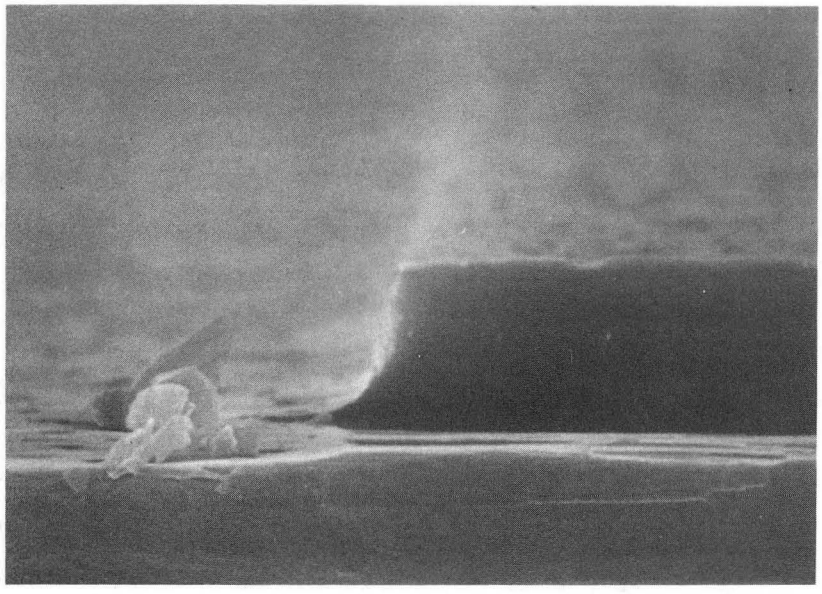

(c) —— 0.741 μm

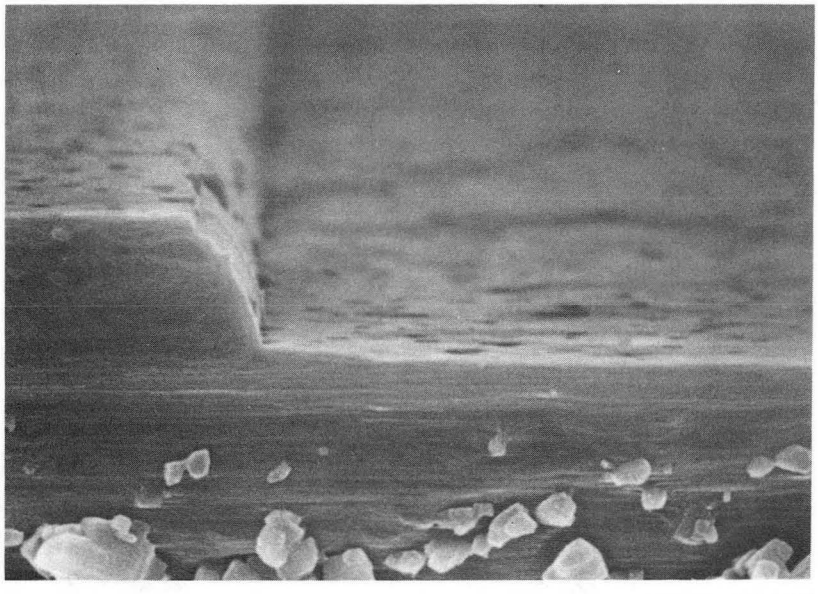

XBB 909-7715

(d) —— 0.741 μm

Figure 10 (cont'd). Initial profiles (c) 10/10 and (d) 10/25, using a 20 min milling time.

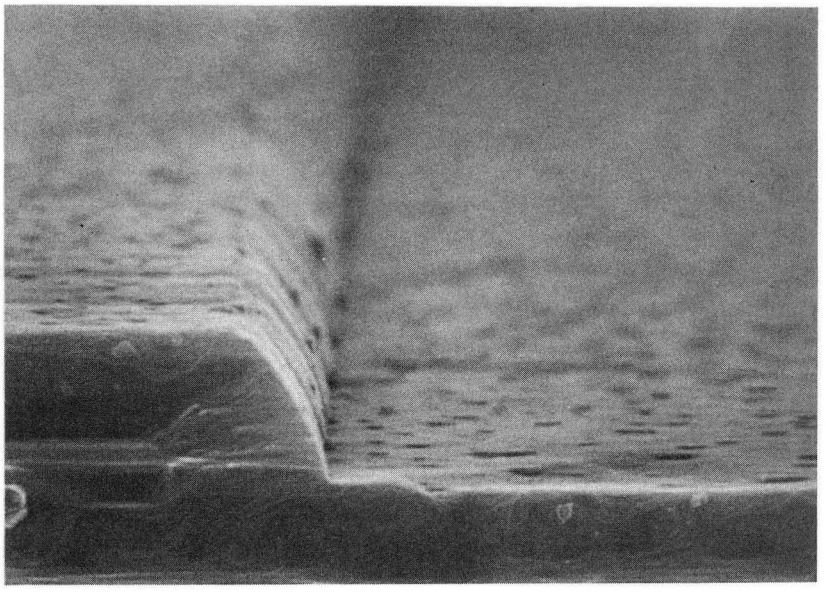

(e) —— 0.741 μm

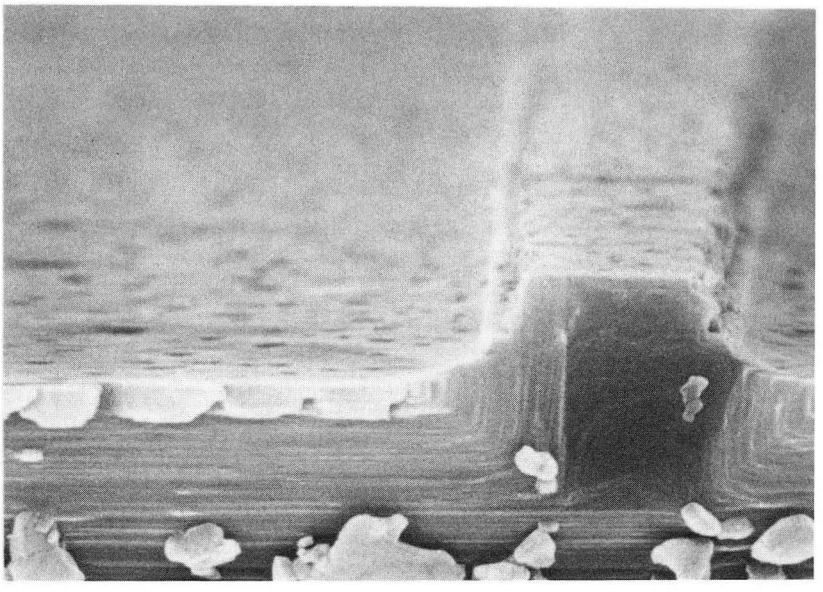

XBB 909-7716

(f) —— 0.741 μm

Figure 10 (cont'd). Initial profiles (e) 10/100 and (f) 25/5, using a 20 min milling time.

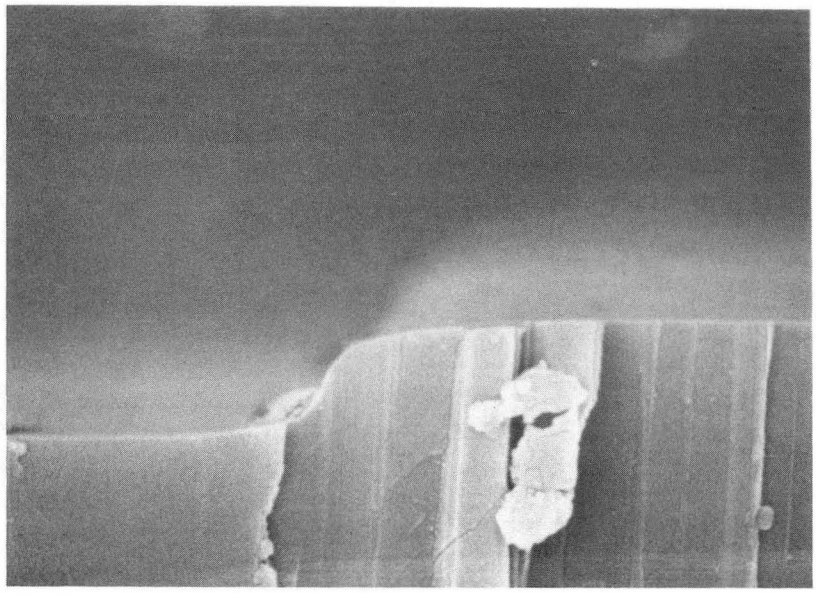

(a) —— 0.741 μm

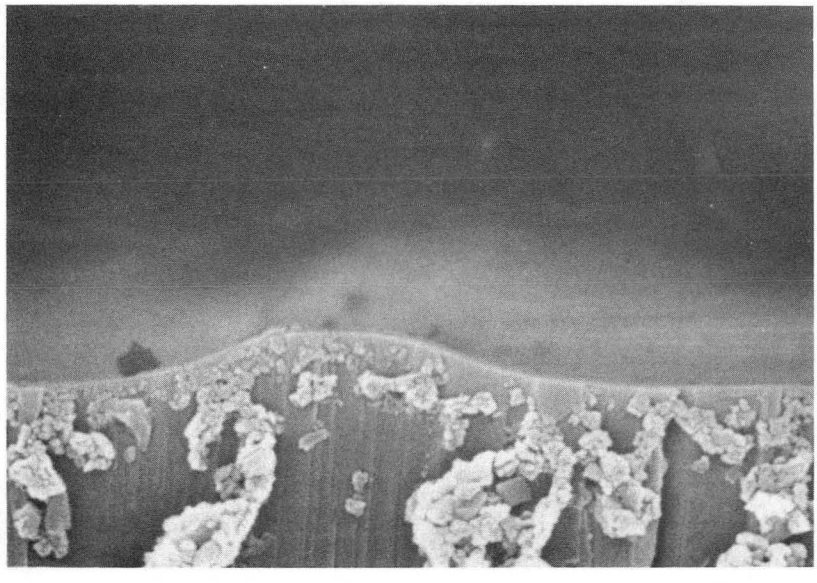

XBB 909-7717

(b) —— 0.741 μm

Figure 11. Profiles of specimens annealed at 770°C for 8 h in argon and then slowly cooled to room temperature. Profiles shown are (a) 5/5 and (b) 5/10.

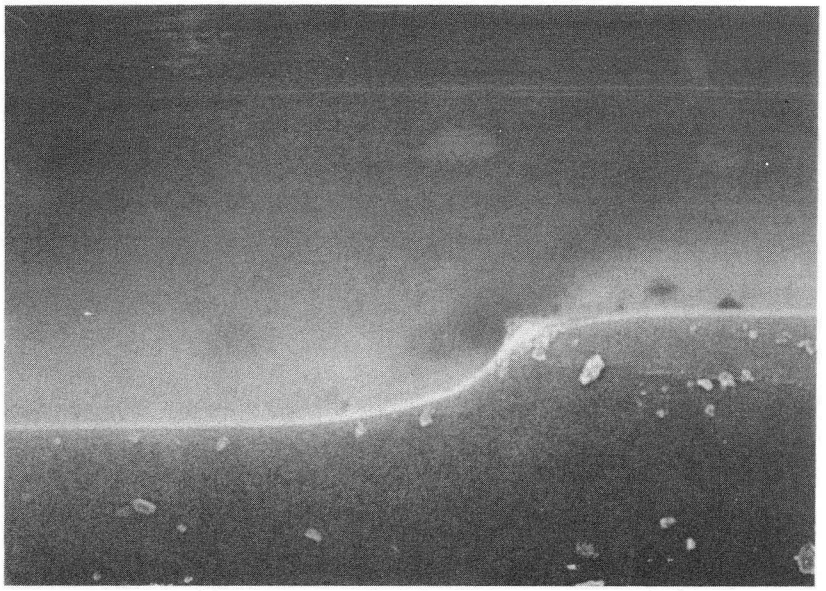

(c) —— 0.741 μm

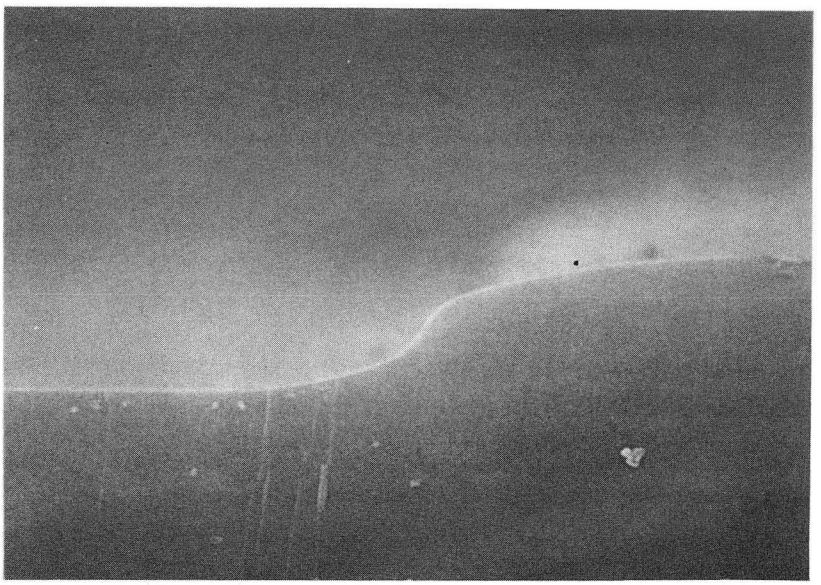

XBB 909-7718

(d) —— 0.741 μm

Figure 11 (cont'd). Profiles of specimens annealed at 770°C for 8 h in argon and then slowly cooled to room temperature. Profiles shown are (c) 10/10 and (b) 10/25.

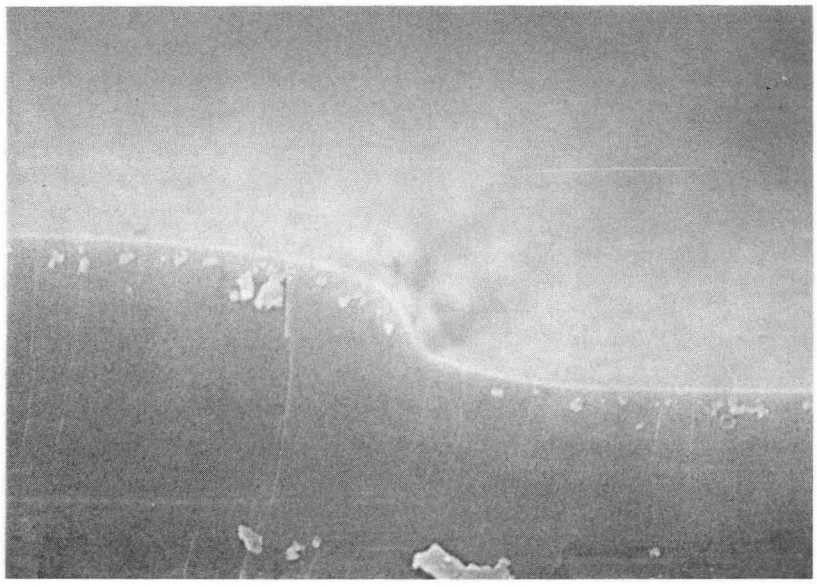

(e) —— 0.741 μm

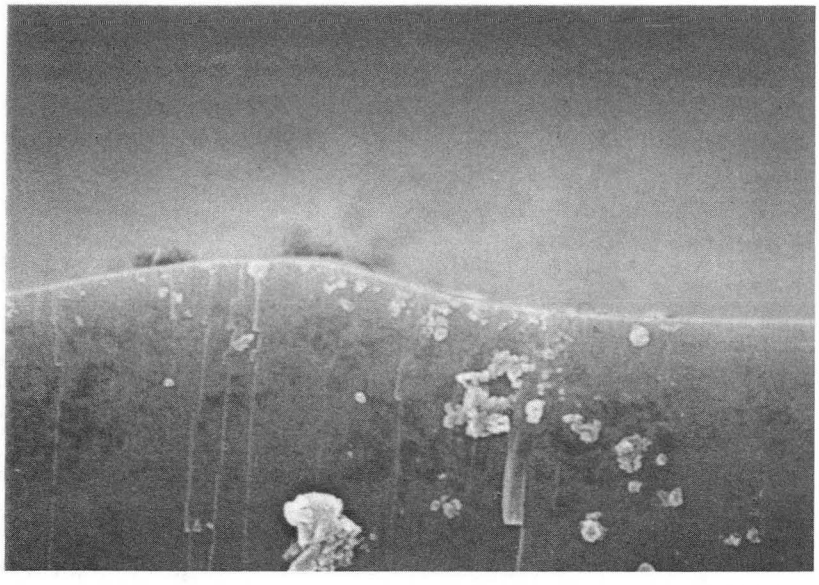

XBB 909-7719

(f) —— 0.741 μm

Figure 11 (cont'd). Profiles of specimens annealed at 770°C for 8 h in argon and then slowly cooled to room temperature. Profiles shown are (e)10/100 and (f) 25/5.

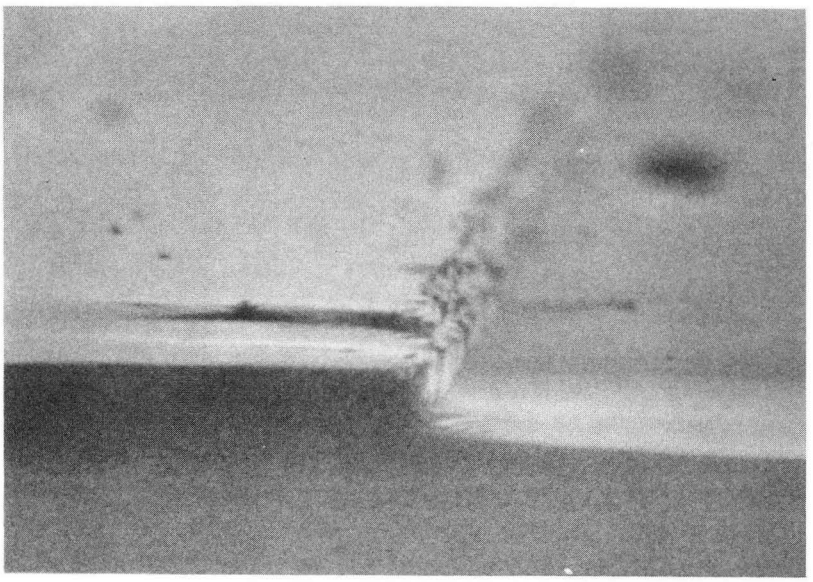

(a) —— 0.781 μm

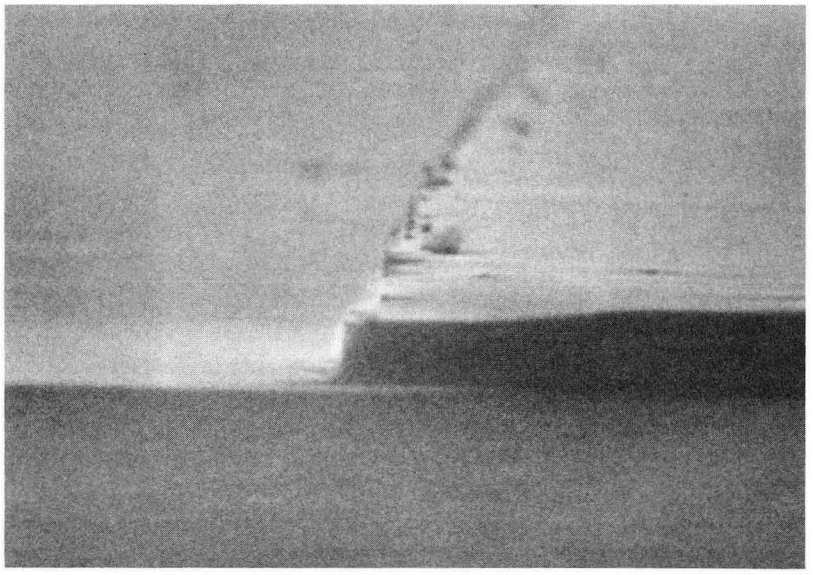

XBB 909-7720

(b) —— 0.781 μm

Figure 12. Profiles of specimens annealed at 770°C for 8 h in argon, slowly cooled to room temperature, then reannealed at 730°C for 16 h in argon and slowly cooled to room temperature.

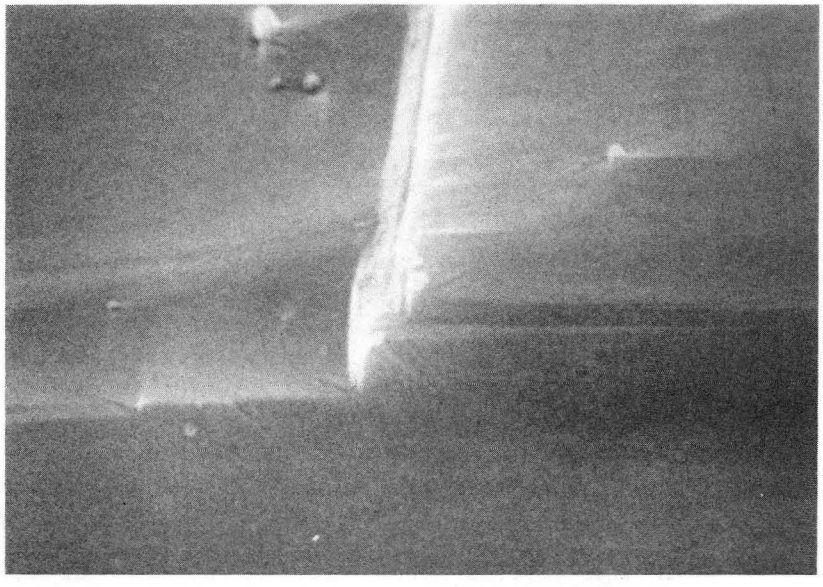

XBB 909-7721

(c) —— 0.714 μm

Figure 12 (cont'd). Profiles of specimens annealed at 770°C for 8 h in argon, slowly cooled to room temperature, then reannealed at 730°C for 16 h in argon and slowly cooled to room temperature.

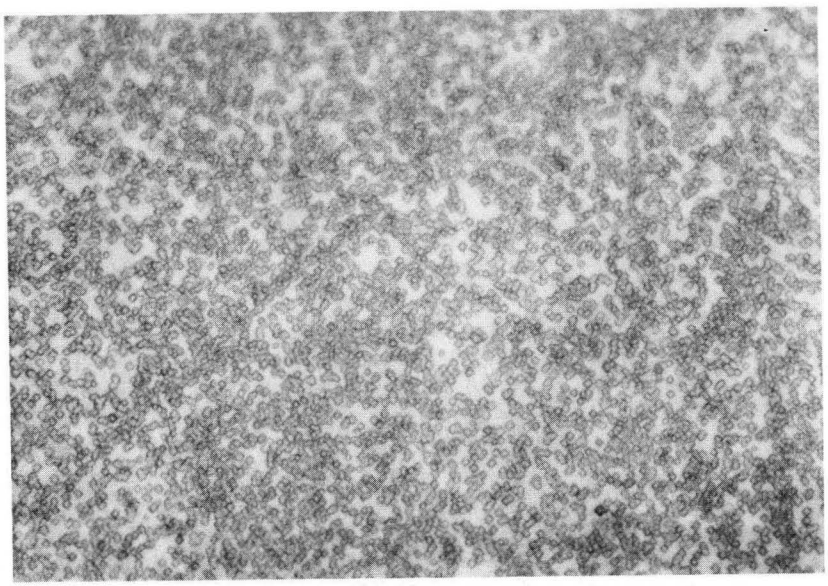

(a) 400 X

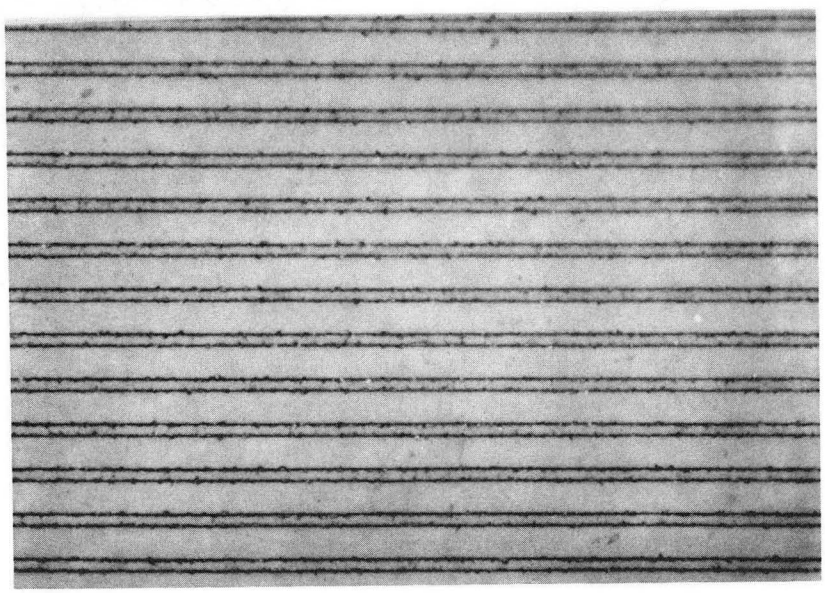

XBB 909-7722

(b) 400 X

Figure 13. (a) Dislocation etch pits formed from etching in CP-4 reagent for 90 s, and (b) a 10/5 profile for scale reference.

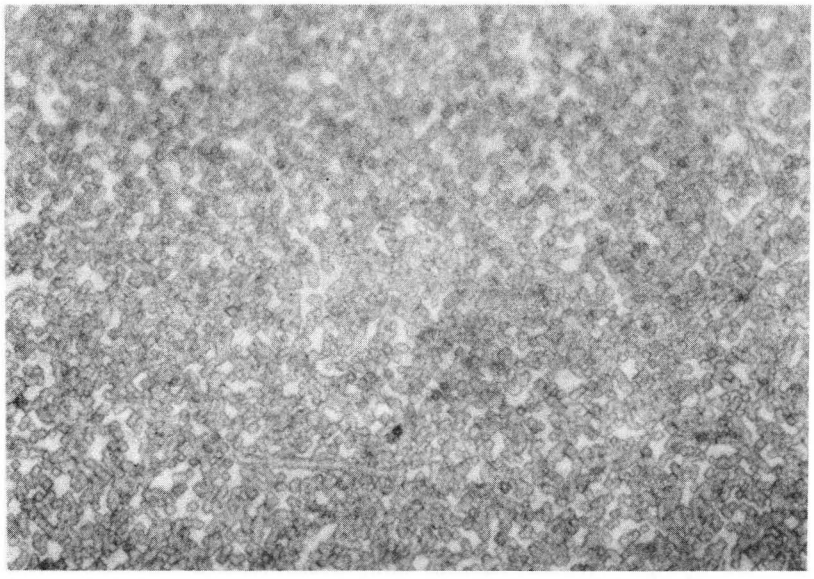

XBB 909-7723

(c) 400 X

Figure 13 (cont'd). Dislocation etch pits formed on the same wafer as in 13(a) but at a different location (refer to 13(b) for scale reference).

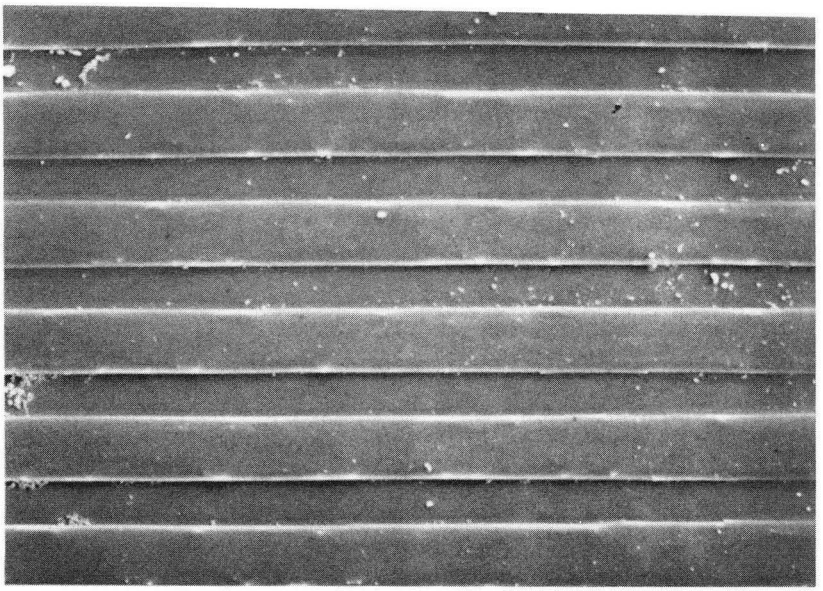

(a) —— 9.62 μm

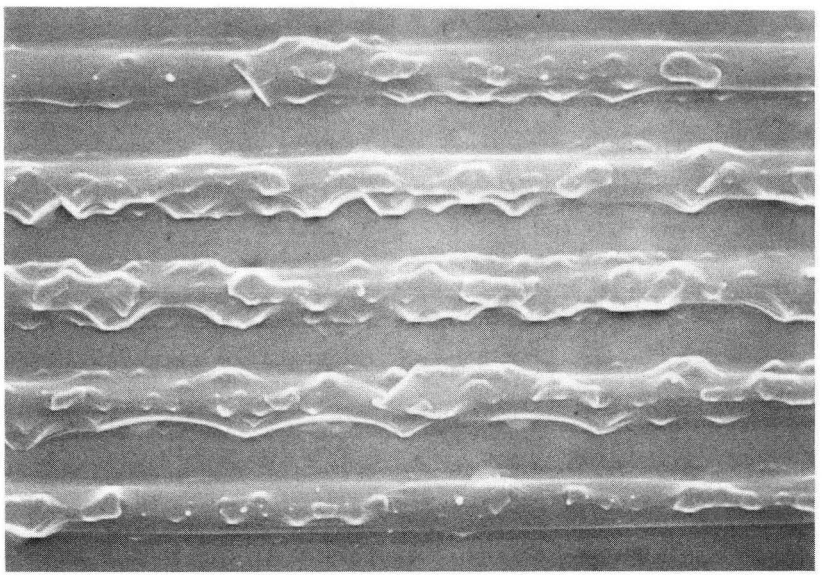

XBB 909-7724

(b) —— 9.62 μm

Figure 14. 5/10 type profile (a) after annealing at 600°C for 15 h in air, and (b) after subsequent annealing at 770°C for 4 h in argon. A 12 min milling time was used.

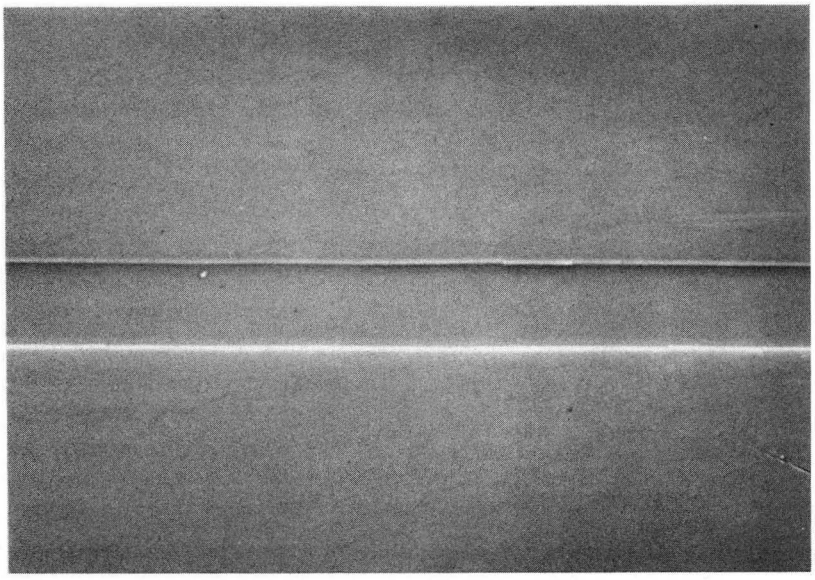

(c) —— 9.62 μm

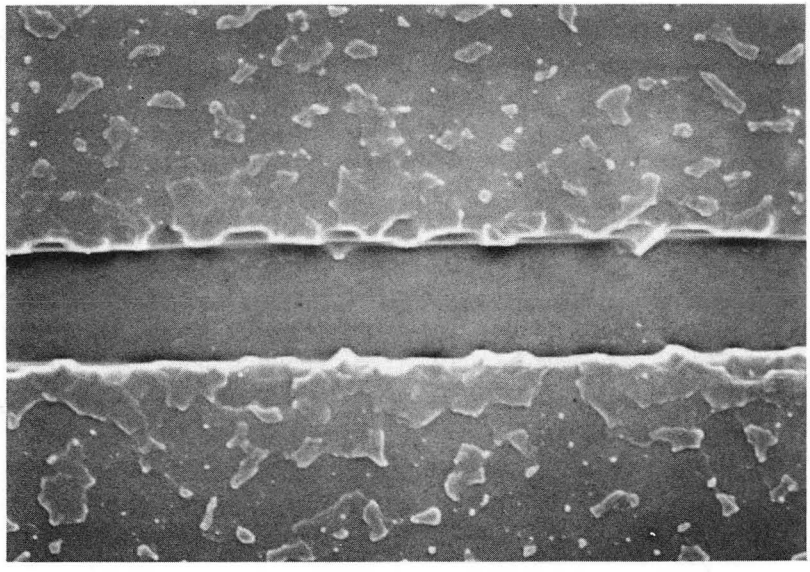

XBB 909-7725

(d) —— 9.62 μm

Figure 14 (cont'd). 10/100 type profile (c) after annealing at 600°C for 15 h in air, and (d) after subsequent annealing at 770°C for 4 h in argon. A 12 min milling time was used.

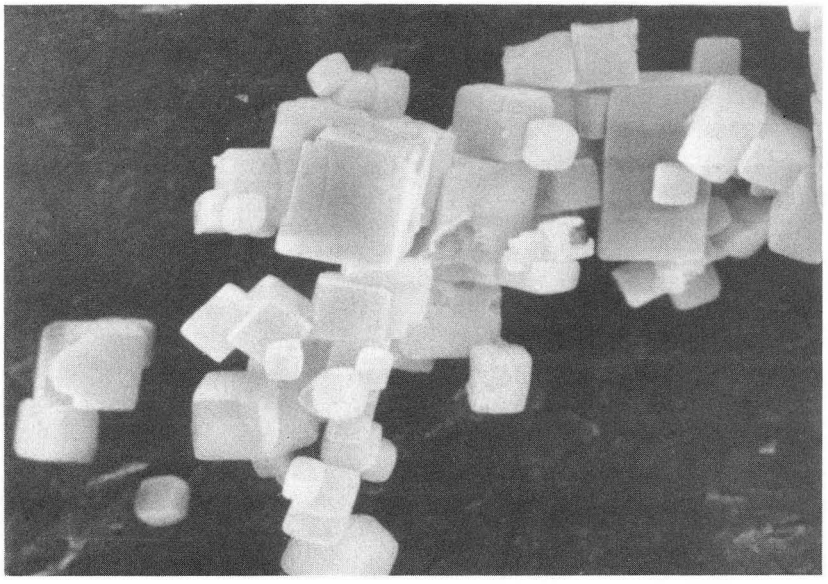

(a) —— 2.20 μm

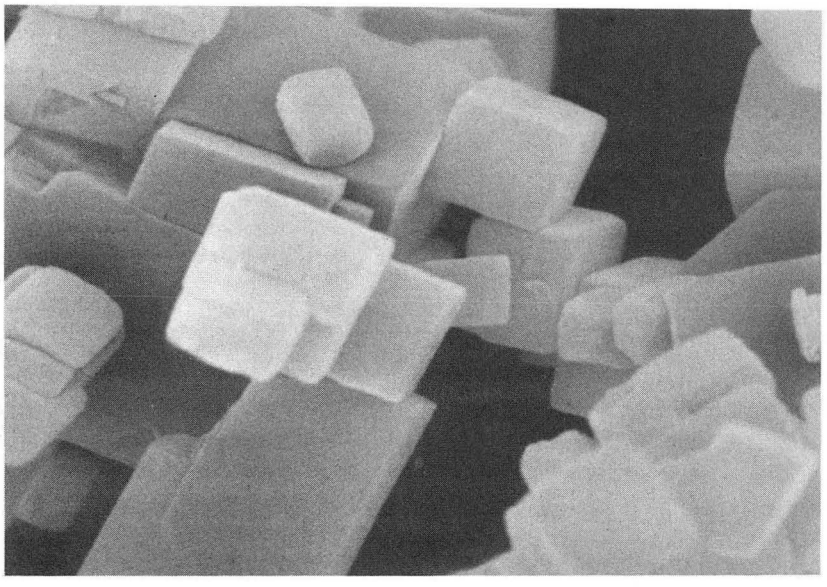

XBB 909-7726

(b) —— 0.943 μm

Figure 15. Initial LiF particles (as received).

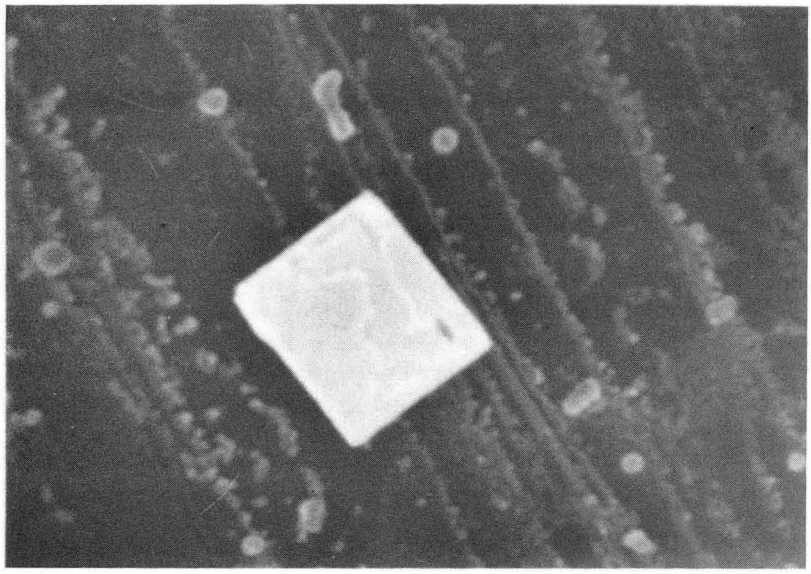

(a) —— 1.08 μm

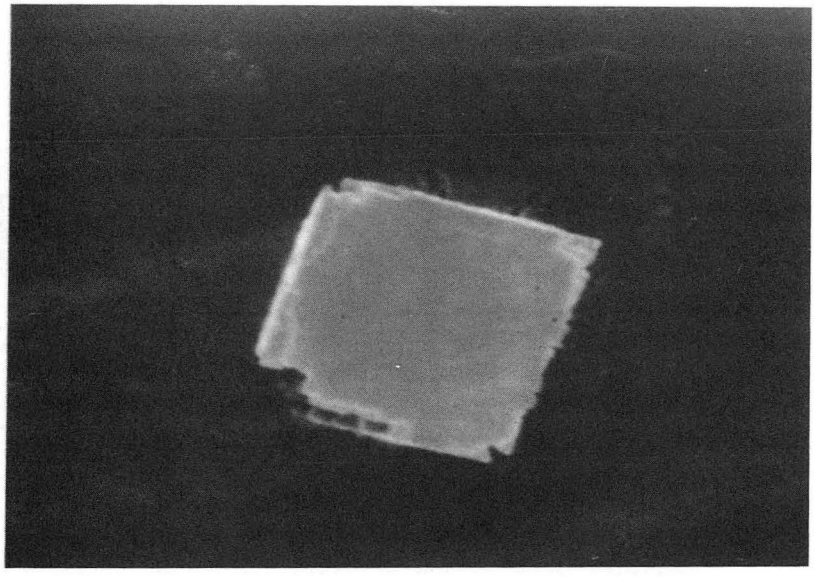

XBB 909-7727

(b) —— 0.637 μm

Figure 16. Isolated LiF particles after dispersion onto a single crystal graphite chip.

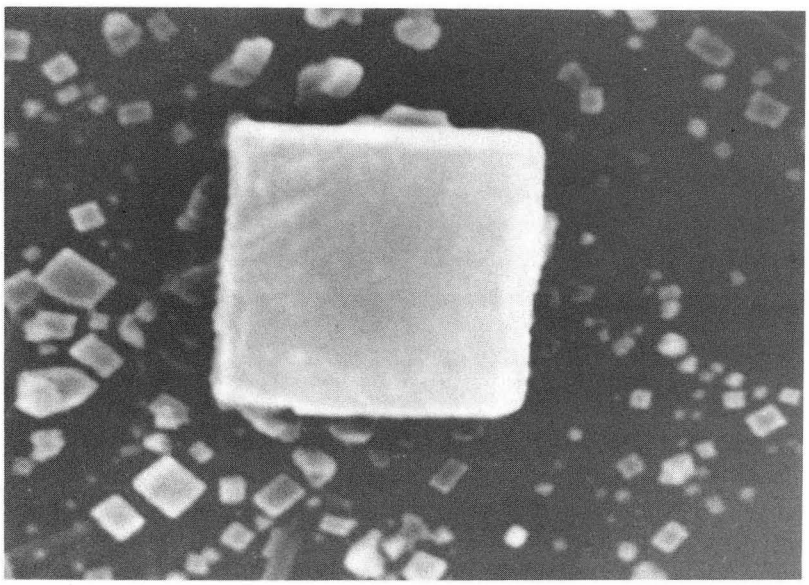

(a) —— 0.541 μm

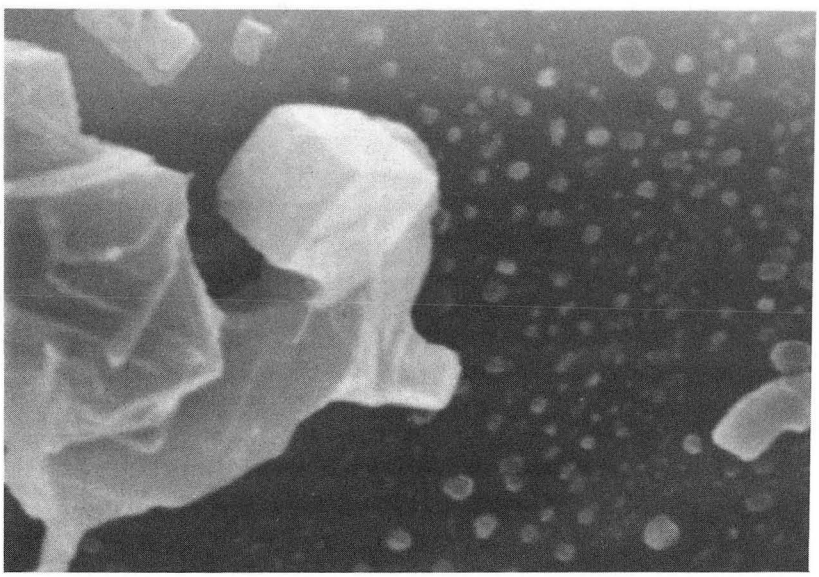

XBB 909-7728

(b) —— 1.06 μm

Figure 17. (a) isolated and (b) clustered LiF particles after annealing at 680°C for 4 h in ~10^{-6} Torr vacuum.

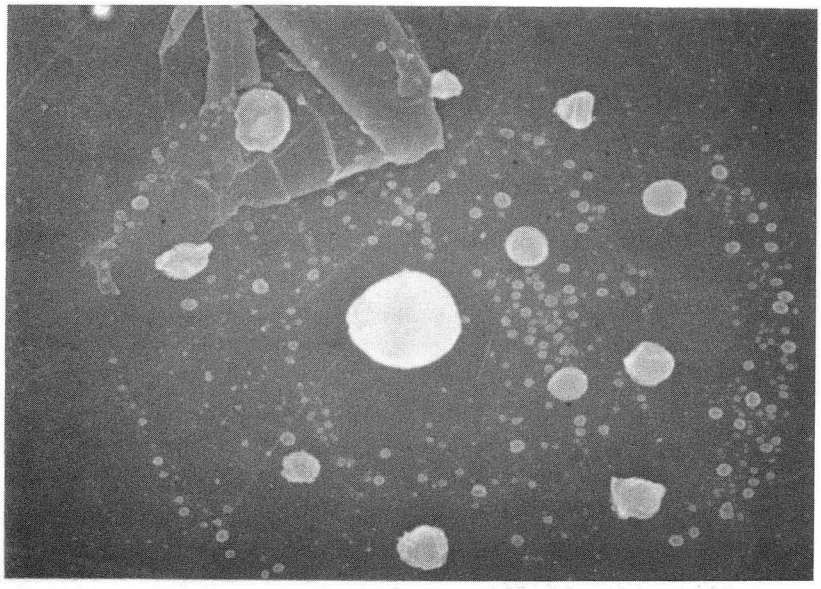

(a) —— 2.20 μm

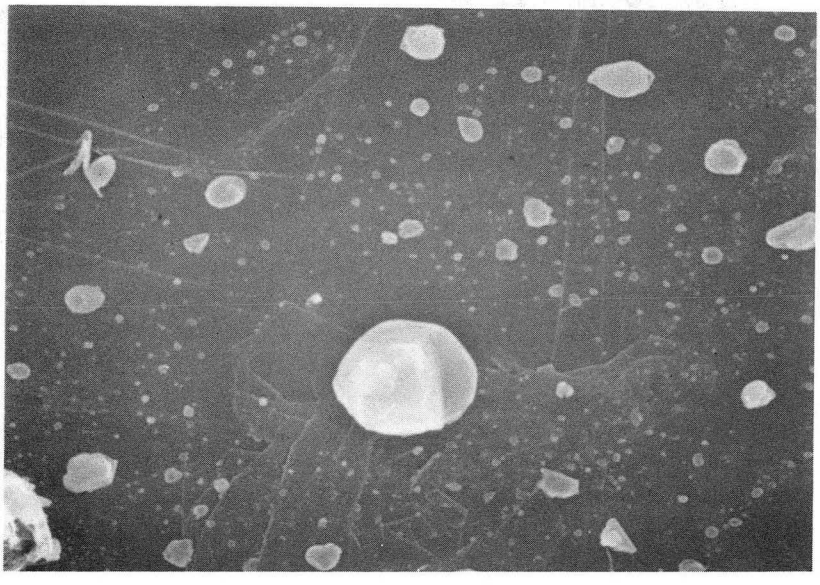

XBB 909-7729

(b) —— 2.20 μm

Figure 18. Isolated particles after annealing at 680°C for 8 h in argon.

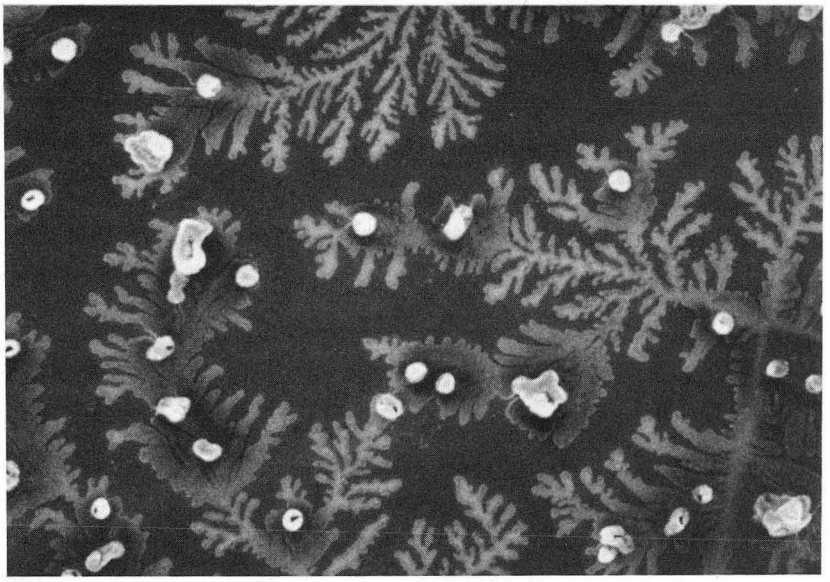

XBB 909-7730

1.18 μm

Figure 19. Ethanol/HCl solution saturated with lithium fluoride, deposited on a single crystal graphite chip and allowed to dry.

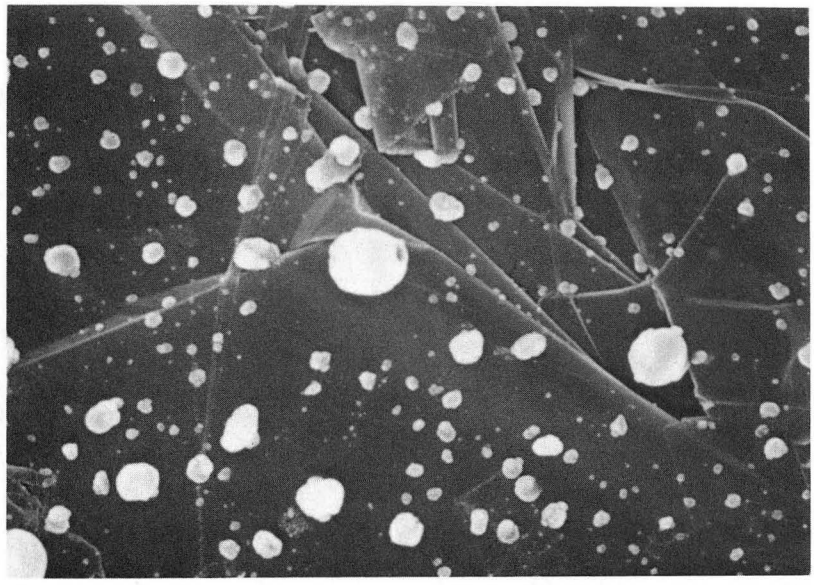

(a) —— 1.18 μm

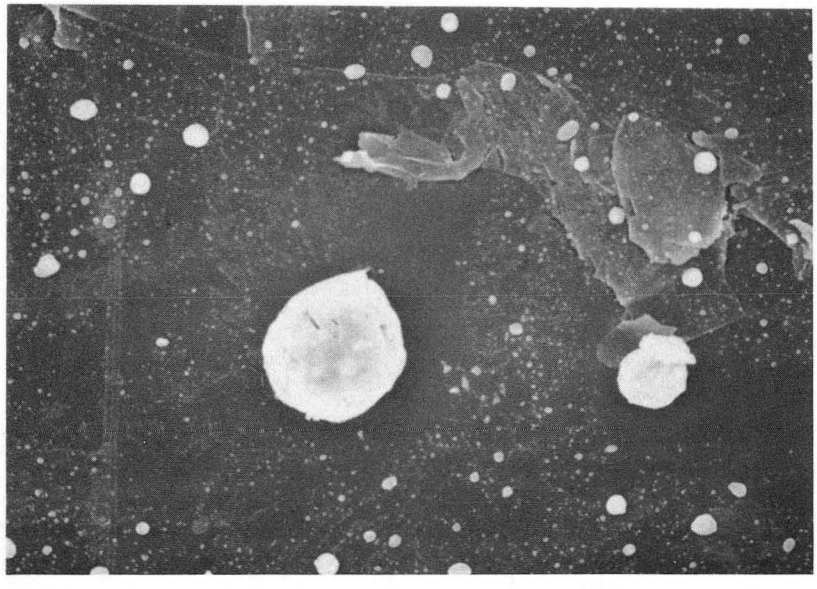

XBB 909-7731

(b) —— 5.92 μm

Figure 20. Particles formed from a dispersion of a saturated suspending solution (see Fig. 17) upon annealing at 680°C for 8 h in argon.

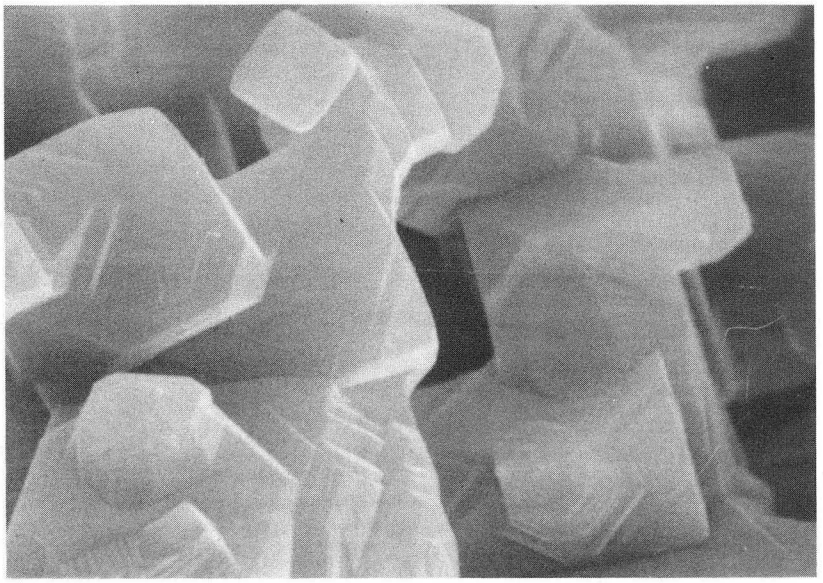

(a) —— 1.00 μm

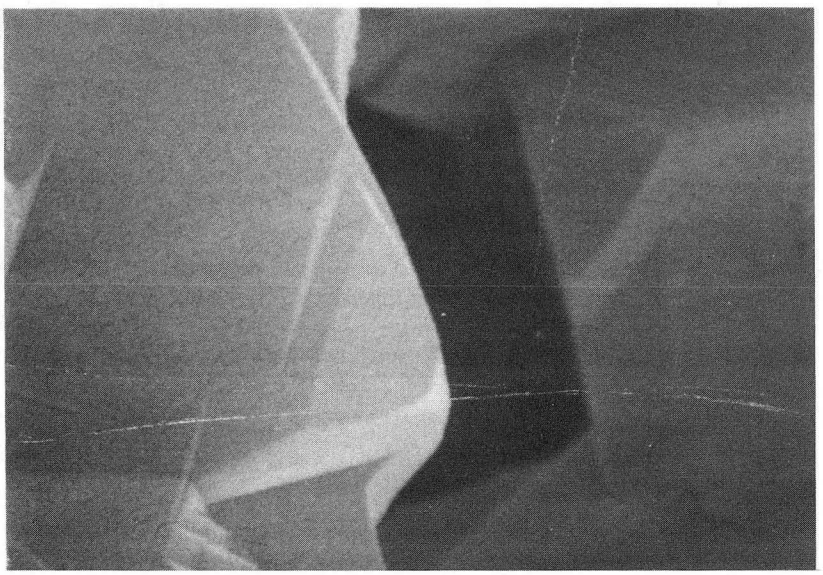

XBB 909-7732

(b) —— 0.400 μm

Figure 21. Bulk LiF powder compact after annealing at 680°C for 8 h in a ~10^{-6} Torr vacuum.

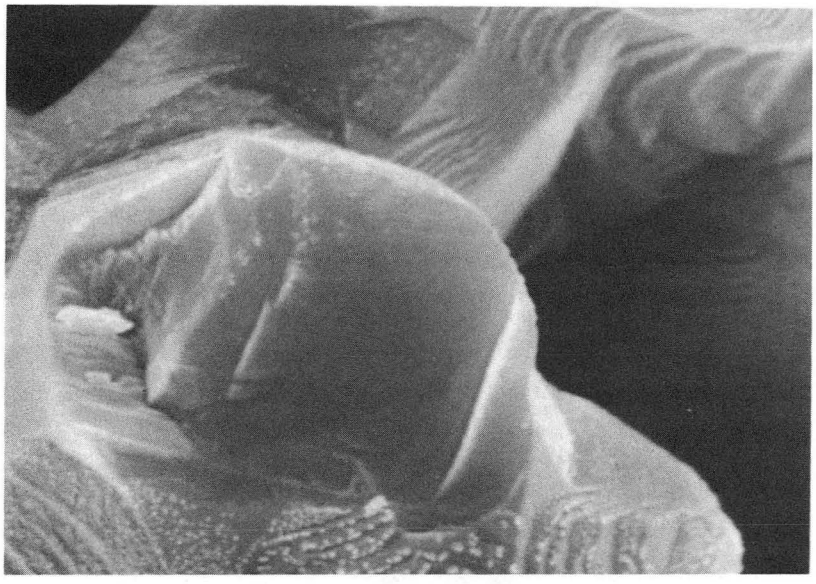

XBB 909-7733

1.22 μm

Figure 22. Bulk LiF powder compact after annealing at 760°C for 4 h in a ~10^{-6} Torr vacuum and allowed to slowly cool to room temperature.

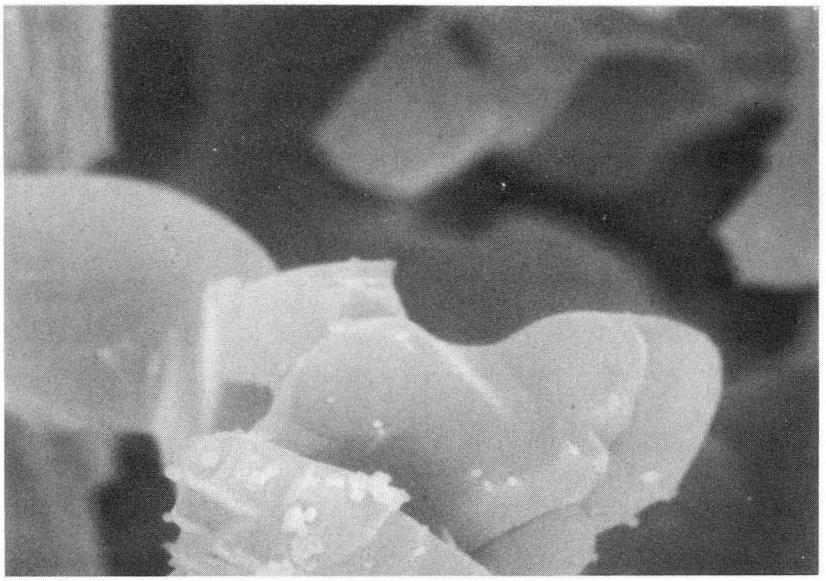

(a) —— 1.22 μm

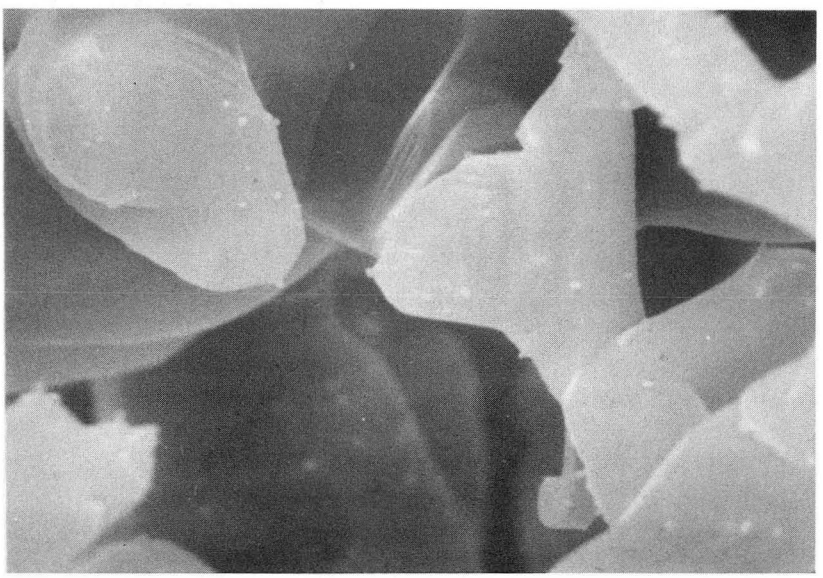

XBB 909-7734

(b) —— 1.22 μm

Figure 23. Bulk LiF powder compact annealed at 760°C for 4 h in a ~10^{-6} Torr vacuum, then quenched to room temperature.

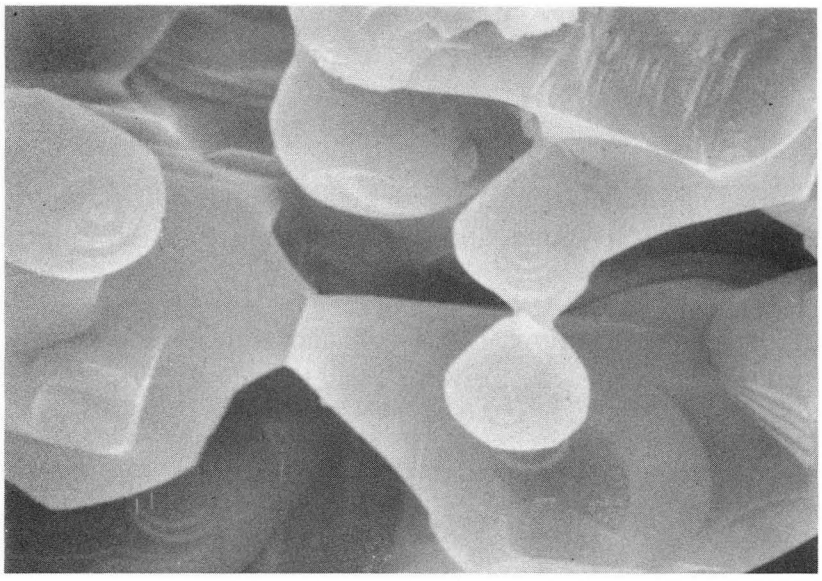

(a) —— 2.22 μm

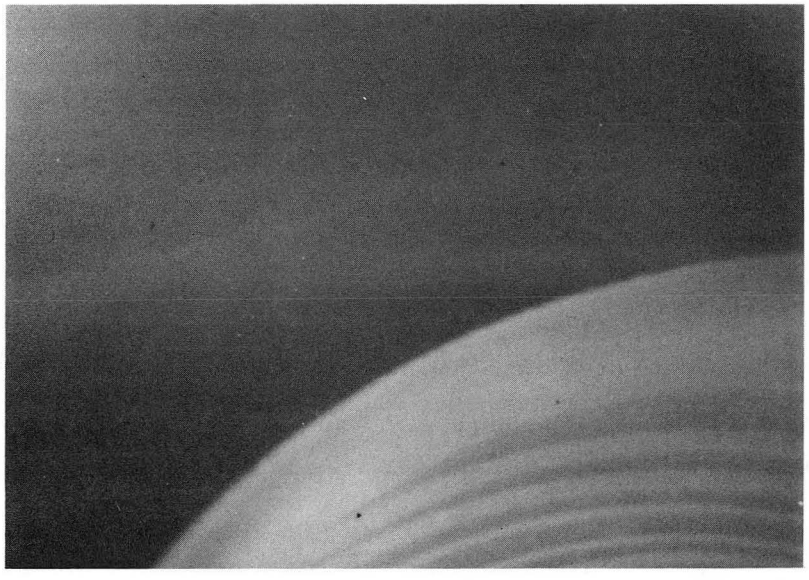

XBB 909-7735

(b) —— 0.333 μm

Figure 24. Bulk LiF powder compact after annealing at 680°C for 8 h in argon.

Endnotes

1. Burke, J.E. **The Chemical and Mechanical Behavior of Inorganic Materials.** Ch. 18. A.W. Searcy, D.V. Ragone, and U. Colombo. Eds. Wiley-Interscience. New York. 1970.

2. Mikijelj, B. and Whittemore, O.J."Grain Cuboidization During Sintering of MgO-$MgCl_2$(1%)". **American Ceramic Society Bulletin.** Vol. 66. No.5 pp. 809-812. 1987.

3. Kim, M.G. et. al."Shape and Size of Crystalline MgO Particles Formed by the Decomposition of $Mg(OH)_2$". **Journal of The American Ceramic Society.** Vol. 71. No. 8. pp.C-373-C-375. 1988.

4. Kingery, W.D. et. al. **Introduction to Ceramics.** 2nd edition. Ch. 10. Wiley-Interscience. New York. 1976.

5. **Fine Ceramics.** S. Saito, Ed. Elsevier. p. 127. 1988.

6. Roedel, J. "The Application of Controlled Interfacial Pore Structures to Pore Perturbation and Pore Drag in Alumina". **Ph.D. Thesis.** Department of Materials Science and Mineral Engineering. University of California, Berkeley, and Lawrence Berkeley Laboratory. 1988.

7. Wang, Z.Y. et. al. "Pore-Grain Boundary Configurations in Lithium Fluoride". **Journal of the American Ceramic Society.** Vol. 69. No. 10. pp. 735-740. 1986.

8. Miller, W.A. et. al."Anisotropy of Interfacial Free Energy of Some Hexagonal Close-packed Metals". **Philosophy Magazine.** Vol. 19. pp. 305-319. 1969.

9. Kirchner, H.O.K. and Chadwick, G.A."Anisotropy of Surface Free Energy of Cadmium and Magnesium". **Philosophy Magazine.** Vol. 20. pp. 405-411. 1969.

10. Roedel, J. and Glaeser, A.M. "High-Temperature Healing of Lithographically Introduced Cracks in Sapphire." **Journal of the American Ceramic Society.** Vol. 73. No. 3. pp. 592-601. 1990.

11. Raj, R. et. al. "On the Sintering Rate of Cleavage Cracks". **Acta Metallurgica.** Vol. 23. No. 3. pp. 399-403. 1975.

12. Bennison, S.J. and Harmer, M.P."Effect of Magnesia Solute on Surface Diffusion in Sapphire and the Role of Magnesia in the Sintering of Alumina". **Journal of the American Ceramic Society.** Vol. 73. No. 4. pp. 833-837. 1990.

13. Gibbs, J.W. "The Collected Works, Vol. 1. Thermodynamics". p. 252. Longmans, Green. New York. 1931.

14. Curie, P. **Bull. Soc. Mineral. Fr.** Vol. 8. p. 145. 1885.

15. Adamson, A.W. **Physical Chemistry of Surfaces.** 4th edition. Ch. 2. pp. 4-6. Wiley-Interscience. 1982.

16. Mullins, W.W. "Solid Surface Morphologies Governed by Capillarity". **Metal Surfaces: Structure, Energetics, and Kinetics.** ASM Seminar. Metals Park, Ohio. pp. 17-65. 1963.

17. Herring, C. "Surface Tension as a Motivation for Sintering". **The Physics of Powder Metallurgy.** pp. 143-179. New York. 1951.

18. Searcy, A.W. "Driving Force for Sintering of Particles with Anisotropic Surface Energies". **Journal of the American Ceramic Society.** Vol. 68. No.10. pp. C-267-C268. 1985.

19. Hoffman, D.W. and Cahn, J.W. "A Vector Thermodynamics for Anisotropic Surfaces-I. Fundamentals and Application to Plane Surface Junctions". **Surface Science.** Vol. 31. pp. 368-388. 1972.

20. Cahn, J.W. and Hoffman, D.W. "A Vector Thermodynamics for Anisotropic Surfaces-II. Curved and Faceted Surfaces". **Acta Metallurgica.** Vol. 22. pp. 1205-1214. 1974.

21. Winterbottom, W.L. "Equilibrium Shape of a Small Particle in Contact with a Foreign Substrate". **Acta Metallurgica.** Vol. 15. pp. 303-310. 1967.

22. Hirth, J.P. and Pound, G.M. **Condensation and Evaporation-Nucleation and Growth Processes.** 1964.

23. Herring, C. **Structure and Properties of Solid Surfaces.** p. 5. 1953.

24. Rottman, C. and Wortis, M."Exact Equilibrium Crystal Shapes at Nonzero Temperature in Two Dimensions". **Physical Review. B.** Vol. 24. No. 11. p. 6274-6277. 1981.

25. Burton, W.K. et. al. "The Growth of Crystals and the Equilibrium Structure of Their Surfaces". **Philosophical Transactions of the Royal Society of London.** Vol. 243. No. 866. pp. 299-358. 1951.

26. Sundquist, B.E. "The Effect of Metallic Impurities and Temperature on the Anisotropy of the Surface Free Energy of Solid Metals". **Acta Metallurgica.** Vol. 12. pp. 585-592. 1964.

27. Sundquist, B.E. "A Direct Determination of the Anisotropy of the Surface Free Energy of Solid Gold, Silver, Copper, Nickel and Alpha and Gamma Iron". **Acta Metallurgica.** Vol. 12. pp. 67-86. 1964.

28. Heyraud, J.C. and Metois, J.J."Equilibrium Shape of Gold Crystallites on a Graphite Cleavage Surface: Surface Energies and Interfacial Energy". **Acta Metallurgica.** Vol. 28. pp. 1789-1797. 1980.

29. Heyraud, J.C. and Metois, J.J. "Surface Free Energy Anisotropy Measurement of Indium". **Surface Science.** Vol. 128. p. 334. 1983.

30. Blakely, J.M. and Mykura, H. "Surface Self Diffusion Measurements on Nickel by the Mass Transfer Method". **Acta Metallurgica.** Vol. 9. pp. 23-31. 1961.

31. Bonzel, H.P. "Surface Diffusion of Metals: A Comparison of Intrinsic and Mass Transfer Measurements". **Chemistry and Physics of Solid Surfaces.** CRC Press. pp. 87-110. 1977.

32. Bonzel, H.P. and Gjostein, N.A. "Surface Self-Diffusion Measurements on Copper". **Physica Status Solidi.** Vol. 25. pp. 209-222. 1968.

33. McLean, M. and Hirth, J.P. "Surface Self-Diffusion on Gold". **Surface Science.** Vol. 12. pp. 177-188. 1968.

34. Hoehne, K. and Sizmann,R. "Volume and Surface Self-Diffusion Measurements on Copper by Thermal Surface Smoothing". **Physica Status Solidi.** Vol. 5. pp. 577-589. 1971.

35. Searcy, A.W. Private communication.

36. Dittmar, W. and Neumann, K."Uber die Gestalt und das Wachstum nadelformiger Kaliumkristalle." **Z. fur Elektrochemie.** Vol. 61. pp. 70-73. 1957.

37. Chou, T.C. and Chou Y.T."Equilibrium Shapes of Ni_3Al Crystallites Formed During Diffusion Anneal". **Journal of Materials Science Letters.** Vol. 4 pp. 1340-1346. 1985.

38. Thompson, R.J. and Munir, Z.A. "Influence of Particle Size on the Sintering Kinetics of Ultrapure Sodium Chloride". **Journal of the American Ceramic Society.** Vol. 65. No. 6. pp. 312-316.

39. Kumar, P. and Johnson, D. "Sintering of CoO". **Journal of the American Ceramic Society.** Vol. 57. No. 2. pp. 62-64. 1974.

40. Gloersen, P.G."Ion Beam Etching". **Journal of Vacuum Science and Technology.** Vol.12. No.1. pp.28-35. 1975.

41. Melliar-Smith, C.M. "Ion Etching for Pattern Delineation". **Journal of Vacuum Science and Technology.** Vol.13. No.5. pp.1008-1022. 1976.

42. Frenken, J.W.M. and van der Veen, J.F."Observation of Surface Melting". **Physical Review Letters.** Vol. 54. No. 2. pp.134-137. 1985.

43. Gilman, J.J. and Johnston, W.G."Observations of Dislocation Glide and Climb in Lithium Fluoride Crystals". **Journal of Applied Physics.** Vol. 27. No. 9. pp. 1018-1022. 1956.

44. Estel, J. et. al."On the Problem of Water Adsorption on Alkali Halide Cleavage Planes, Investigated by Secondary Ion Mass Spectroscopy". **Surface Science.** Vol. 54. pp. 393-418. 1976.

45. Brailsford, A.D. and Gjostein, N.A."Influence of Surface Energy Anisotropy on Morphological Changes Occurring by Surface Diffusion". **Journal of Applied Physics.** Vol. 46. No. 6. pp.2390-2397. 1975.

LAWRENCE BERKELEY LABORATORY
UNIVERSITY OF CALIFORNIA
INFORMATION RESOURCES DEPARTMENT
BERKELEY, CALIFORNIA 94720